수의학 석사학위 논문

고콜레스테롤이 유도하는 중간엽 줄기세포 자멸사에 대한 멜라토닌의 보호 효과

Protective effects of melatonin on high-cholesterol-induced apoptosis of mesenchymal stem cells

2020년 8월

서울대학교 대학원

수의학과 수의생명과학 전공
(수의생리학)

김 준 성

ABSTRACT

Protective effects of melatonin on high-cholesterol-induced apoptosis of mesenchymal stem cells

Jun Sung Kim

Major in Veterinary Biomedical Science

Department of Veterinary Medicine

The Graduate School

Seoul National University

High cholesterol levels of patients with obesity are associated with insufficient efficacy of transplantation therapy using umbilical cord blood-derived mesenchymal stem cells (UCB-MSCs). Further, the regulation of intracellular cholesterol levels is important for reducing apoptosis of engrafted donor stem cells. The endogenous hormone melatonin contributes to the prevention of cholesterol accumulation in patients with obesity through a poorly understood mechanism. Therefore, this study investigated the regulatory mechanism of melatonin that inhibits cholesterol-induced apoptosis in vitro and in

vivo. Melatonin increased the expression of ATP-binding cassette subfamily A member 1 (ABCA1) in UCB-MSCs, which reduced cholesterol accumulation and cholesterol-induced apoptosis. In addition, pretreatment with disodium 4,4′-diisothiocyanatostilbene-2,2′-disulfonate (DIDS), an ABCA1 inhibitor, diminished these effects. Skin wound healing to show that melatonin treatment restored the survival rate of transplanted UCB-MSCs and wound-healing capacity, which was lowered in high-fat-diet-induced obese mice. In the presence of high concentrations of cholesterol, melatonin receptor 2 (MT2) level increased, and melatonin treatment inhibited the expression of binding immunoglobulin protein (BiP) through regulation of the MT2/Sp1-dependent microRNA-597. Melatonin decreased co-localization of BiP with nuclear factor erythroid 2-related factor 1 (NRF1), which is required for the translocation of NRF1. Inhibition of the nuclear translocation of NRF1 increased ABCA1 expression and cholesterol efflux and inhibited apoptosis in the presence of high cholesterol concentrations. In conclusion, these findings indicate that melatonin induced the efflux of intracellular cholesterol through ABCA1 to decrease the apoptosis of UCB-MSCs in the presence of high cholesterol concentrations through an MT2-dependent BiP/NRF1 pathway.

Keywords: Melatonin, Mesenchymal stem cell transplantation, Cholesterol, BiP, NFE2L1, ABCA1

Student Number: 2016-21752

CONTENTS

LIST OF FIGURES

LIST OF TABLES

ABBREVIATIONS

NRF1	nuclear factor erythroid 2-related factor 1
ABCA1	ATP-binding cassette subfamily A member 1
HRD1	HMG-CoA reductase degradation 1
ERAD	endoplasmic-reticulum-associated degradation
BiP	binding immunoglobulin protein
SEL1L	sel-1 homolog 1
UCB-MSCs	umbilical cord blood-derived mesenchymal stem cells
ROS	reactive oxygen species
4-P-PDOT	4-phenyl-2-propionamidotetralin
DIDS	disodium 4,4′-diisothiocyanatostilbene-2,2′-disulfonate
α-SMA	alpha-smooth muscle antigen
MT1	melatonin receptor 1
MT2	melatonin receptor 2
miR	microRNA
PBS	phosphate-buffered saline
TBST	tris-buffered saline containing Tween-20
RT	room temperature
NGS	normal goat serum
SRRF	super-resolution radial fluctuations

siRNA	small interfering RNAs
NT	non-targeting
qPCR	quantitative polymerase chain reaction
PI	propidium iodide
WST	water-soluble tetrazolium
HFD	high-fat diet
ND	normal diet
NS	not significant
PFA	paraformaldehyde
H&E	hematoxylin and eosin
PBST	phosphate-buffered saline containing Tween-20
ANOVA	analysis of variance
RFU	relative fluorescence units
HNA	human nuclear antigen
Sp1	specificity protein 1

INTRODUCTION

The endogenous indoleamine hormone melatonin (N-acetyl-5-methoxytryptamine) is synthesized and secreted by many organs, including the pineal gland that regulates the day□night sleep cycle (Kennaway & Wright, 2002). Melatonin regulates cell physiology, including processes such as the regulation of oxidative stress, cell migration, and apoptosis (Lee et al., 2018b; Lee et al., 2014; Zhu et al., 2019). Moreover, melatonin and cholesterol levels are associated with obesity (Altunkaya et al., 2018; Baron et al., 2017; Karamitri & Jockers, 2019), and melatonin lowers cholesterol absorption and accumulation in rats and mice (Hussain, 2007; Sener et al., 2004). Further, melatonin inhibits the activation of sterol regulatory element-binding transcription factor-1c, fatty acid synthase, and stearoyl-CoA desaturase 1-associated lipogenesis while increasing peroxisome proliferator-activated receptor-α-dependent lipolysis (Chen et al., 2011; Mi et al., 2018). However, the mechanism through which melatonin regulates the efflux of intracellular cholesterol efflux is unknown.

Nuclear factor erythroid 2-related factor 1 (NRF1, NFE2L1) is required to maintain cholesterol homeostasis through repression of the expression of ATP-binding cassette subfamily A member 1 (ABCA1) (Widenmaier et al., 2017). NRF1, which is a member of the cap'n'colar basic leucine zipper family, resides in the endoplasmic reticulum (ER) membrane and the nuclear translocation of NRF1 is stringently regulated by HMG-CoA reductase degradation 1 (HRD1)-dependent ER-associated degradation (ERAD) (Sykiotis &

Bohmann, 2010). The cholesterol recognition/interaction amino acid consensus sequence domain of NRF1 directly binds to cholesterol in the ER membrane, which influences the suppression of HRD1-dependent ERAD and the nuclear translocation of NRF1 (Widenmaier et al., 2017). The substrate of ERAD is recognized by proteins such as binding immunoglobulin protein (BiP), OS9 ER lectin, and store-operated calcium entry associated regulatory factor. These proteins bind to protein sel-1 homolog 1 (SEL1L), the core of the HRD1 complex, to transfer the substrate to HRD1 (Preston & Brodsky, 2017). Elevated concentrations of cholesterol downregulate NRF1 ubiquitination and degradation through ERAD to achieve cholesterol efflux, although the detailed mechanism through which cholesterol regulates ERAD processing of NRF1 is poorly understood (Widenmaier et al., 2017). Moreover, melatonin contributes to ERAD, which leads to the suppression of tunicamycin-induced ER stress as well as senescence (Choi et al., 2017; Fang et al., 2018). These findings indicate that melatonin regulates the mechanism of ERAD-dependent NRF1 translocation that mediates the efflux of high levels of cholesterol.

Clinical reports indicate that the wound healing process for some obese patients is extremely slow, contributing to a higher risk of infection and diminished quality of life (Avishai et al., 2017; Guo & Dipietro, 2010). Besides, metabolic diseases such as obesity increase the reactive oxygen species (ROS), and consequently, induces a delay in vasculogenesis, granulation and re-epithelialization of wound sites (Masson-Meyers et al., 2020). Further, rat given a high-fat diet showed delayed wound healing, which seems to be related to oxidative stress environment (Nascimento & Costa, 2006). To manipulate the obese-related

wound, multiple promising therapies using stem cells are currently under investigation. Umbilical cord blood-derived mesenchymal stem cells (UCB-MSCs) have low immunity and immunomodulatory effects, whch can increase the survival of transplanted cells and decrease the risk of Graft-versus-host disease (Zhao et al., 2019). Therefore, UCB-MSCs can be used for specific cell-based therapies, such as cerebral ischemia, Parkinson's disease, Alzheimer's disease, multiple sclerosis, retinal disease, type 1 and 2 diabetes, and myogenic disease (Naji et al., 2019). Further, UCB-MSCs are widely used to accelerate tissue regeneration because of their ability to self-renew, mediate the paracrine effects of immunomodulatory and vasculogenetic cytokines, and differentiate into diverse cell lineages (Strong et al., 2017). However, the therapeutic efficacy of stem cell transplantation to treat patients with obesity accompanied by hyperlipidemia and hypercholesterolemia is lower than that achieved for treating patients who are not obese (Awad et al., 2005; Jung et al., 2018; Veghari et al., 2013). High levels of circulating cholesterol increase its intracellular levels, and excess cholesterol induces ER stress, the production of NADPH oxidase-dependent ROS, and oxidative stress of sufficient intensity to cause cell death (Feng et al., 2003; Kedi et al., 2009; Tabas, 2004). Further, the cholesterol transporter is closely associated with the levels of intracellular cholesterol and ROS as well as apoptosis when cells are exposed to high concentrations of cholesterol (Hsu et al., 2018; Yvan-Charvet et al., 2010). Considering that excessive intracellular cholesterol increases cell death and that melatonin regulates cholesterol levels, the investigation into the cholesterol regulatory mechanism of melatonin can suggest the possibility of the improved therapeutic effects of UCB-MSCs for treating of skin wound healing in obese

patients. For this purpose, I conducted *in vivo* and *in vitro* studies of UCB-MSCs to identify the regulatory mechanism and effects of melatonin on intracellular cholesterol levels and cholesterol-induced apoptosis.

MATERIALS AND METHODS

1. Materials

The UCB-MSCs were acquired from Kang Stem Biotech (Seoul, Korea). Fetal bovine serum (FBS) and antibiotics were purchased from Hyclone (Logan, UT, USA) and Gibco (Grand Island, NY, USA) respectively. 4-P-PDOT (#SML1189), Cholesterol (#C4951), DIDS (#D3514), Melatonin (#M5250), and Ver155008 (#SML0271) were purchased from Sigma-Aldrich (St.Louis, MO, USA), while Mithramycin A (#1489) was purchased from Tocris (Minneapolis, MN, USA). Antibodies for ABCA1 (#ab18180), α-SMA (#ab5694), and Sp1 (#ab227383) were purchased from Abcam (Cambridge, England) and HSF1 (#H00003297-A01) antibody was purchased from Abnova (Taipei, Taiwan). Antibodies for NRF1 (#8052S), and Cleaved-caspase 3 (#9661) were purchased from Cell Signaling Technology (Beverly, MA, USA), while BiP (#MA5-27686) and phospho-Sp1 (Thr453, #PA5-38333) antibodies were purchased from Invitrogen (Carlsbad, CA, USA). Antibodies for MT1 (#NBP1-71113) was purchased from Novus Biologicals (Littleton, CO, USA) and β-actin (#sc-47778), Caspase 9 (#sc-8355), Lamin A/C (#sc-20681), and MT2 (#sc-28453) were purchased from Santa Cruz Biotechnology (Dallas, TX, USA). The mRNA primers for *ABCA1, ABCG1, ABCG5, ABCG8, BIP, DERLIN, HERP, SEL1L, VCP, MT1, MT2* and the miRNA primers for miR-16-5p, miR-181a-5p, miR-3121-3p, miR-495-3p, miR-5688, miR-597-5p and miR-627-3p were purchased from Cosmogenetech (Seoul, Korea). Small

interfering RNAs (siRNAs) for NRF1 and Non-targeting (NT) siRNA were purchased from Bioneer (Deajeon, Korea). All reagents used in these experiments were commercial prepared and highly purified products.

2. Cell cultivation

The UCB-MSCs were cultured with α-minimum essential medium (α-MEM; Hyclone, #SH30265.01), 10% FBS and 1% of antibiotics at 37℃ with 5% CO2. Cells grown to 80% confluency were incubated with serum-free α-MEM for 24 h prior to reagent treatment.

3. Cholesterol quantification assay

The cholesterol quantification was performed according to the manufacture's protocol (Sigma Aldrich, #CS0005). Cells were cultivated in 60 mm size culture dish and after serum-free starvation during 24 h, disodium 4,4′-diisothiocyanatostilbene-2,2′-disulfonate (DIDS), melatonin, or Ver155008 were pretreated before cholesterol treatment. Cells were harvested and cholesterol was extracted with 200 μL of chloroform:isopropanol:NP40 (7:11:0.1) solution. After spun down for max speed to remove debris, the supernatant was transferred to new tubes and dry at 50℃ for 4 h. The pellets were resolved in assay buffer and incubated with enzyme mixed assay buffer at 37℃ for 30 min. Then, the absorbance was measured with a microplate spectrophotometer (Epoch 2™; BioTek, Winooski, VT, USA) at 570 nm.

4. Western blot analysis

Cells were washed in ice-cold phosphate-buffered solution (PBS; Hyclone, #SH30256) twice and harvested with a cell scraper and collected by centrifugation (13,000 rpm, 4℃, 10 min). Cells were lysed with RIPA lysis buffer (Atto, Tokyo, Japan, #AE6500) with provided protease and phosphatase inhibitors. Cell debris was removed by centrifugation (13,000 rpm, 4℃, 10 min). The concentrations of proteins were determined by a bicinchoninic acid protein quantification assay (Thermo Fisher, Waltham, MA, USA, #23227). Samples with equal concentration of proteins were boiled at 100℃ for 10 min with sample buffer. Finally, protein samples were loaded into 8□12% SDS-polyacrylamide gels and transferred to polyvinylidene fluoride membranes (Pall Corporation, New York, USA, #bsp0161). The membranes were washed with tris-buffered saline containing 0.2% Tween-20 (TBST) (10 min, 3 times). The membranes were blocked with 5% skim milk (Gibco, Grand Island, NY, USA, #232100) in TBST at room temperature (RT) for 30 min. After 3 times of TBST washing, the membranes were incubated with a primary antibody solution in TBST (1:2,000 dilution) at 4℃ overnight. After 3 times of washing with TBST, the membrane was incubated with anti-mouse or rabbit horseradish peroxidase-conjugated secondary antibody solution (Invitrogen, #G-21040, #G-21234, 1:10,000 dilution in TBST) at RT for 2 h. Blots were detected with a Clarity Western ECL Substrate kit (Bio-Rad, Hercules, CA, USA, #1705061). The membranes were washed with stripping buffer (1.5% glycine, 0.2% SDS, 1% Tween-20, pH 2.2) for 40 min to reprove loading control bands. The band of β-actin was used as loading control. Collected images of bands were analyzed

with the ImageJ software (National Institutes of Health, Bethesda, MD, USA; imagej.nih.gov./ij/).

5. Immunocytochemistry analysis

UCB-MSCs were cultivated in confocal dishes (SPL, Pocheon, Korea, #200350) and cells at 70% of confluency incubated with serum-free media before experimental treatments. Cells were washed twice with PBS and fixed with 70% Acetone in PBS for 10 min, and then permeabilized with 0.1% TritonX-100 in PBS for 10 min. The cells were incubated with 5% of Normal Goat Serum (NGS, Vector, Germany, #S-1000-20) in PBS solution for 30 min to block background. Cells were incubated with primary antibodies in 5% NGS solution (1:100 dilution) at 4℃ overnight and washed with PBS 3 times. Cells were incubated with Alexa Fluor™ 488 or 555-conjugated secondary antibodies in 5% NGS solution (1:200 dilution) at RT for 2 h. The cells were visualized by super-resolution radial fluctuations (SRRF) imaging system (Andor Technology, Belfast, UK) (Gustafsson et al., 2016). Relative fluorescence intensities of nuclear NRF1, and total NRF1 or co-localization of NRF1 and BiP were quantified with the Fiji software (Schindelin et al., 2012).

6. Transfection of siRNAs or microRNA mimics

25 nM of NRF1 siRNAs or microRNA-597 (miR-597) mimics were incubated with transfection reagent TurboFect™ (Thermo Fisher, #R0531) and transfected to UCB-MSCs for 24 h. The medium was changed to α-MEM with 1% antibiotics prior to the cholesterol treatment. NT siRNA or NT mimic were used as inner control. The sequences of the siRNAs and microRNA mimics used in this study

are described in Table 1.

Table 1. siRNA and microRNA mimic sequences

	Sequence
NRF1 sense	GAGAACGGACGACCCUACU
NRF1 antisense	AGUAGGGUCGUCCGUUCUC
Non-targeting sense	UAGCGACUAAACACAUCAA
Non-targeting antisense	UUGAUGUGUUUAGUCGCUA
hsa-miR-597 mimic	UGUGUCACUCGAGACCACUG U

7. Quantitative polymerase chain reaction (qPCR) for analyzing mRNA and microRNA

Total RNA samples were extracted using RNA extraction kits (Takara, Otsu, Shiga, Japan, #9767). Then, 1 μg of RNA was reverse-transcripted into cDNA with oligo dT primers with reverse transcription-PCR premix (iNtRON Biotechnology, Seongnam, Korea, #25081). The cDNA samples of mRNA were amplified with TB™ Green Premix Ex Taq™ (TaKaRa, #RR420A) and the mRNA primers for target genes. Total RNA samples for microRNA quantitation were extracted by miRNeasy mini kit (Qiagen, Hilden, Germany, #217004). 0.5 μg of RNA was reverse-transcripted into cDNA by miRNA reverse transcription kit (Qiagen, #218160). The cDNA samples were amplified with the forward primers for target microRNAs and universal reverse primer of miScript SYBR Green PCR Kit (Qiagen, #218073). The relative expression levels of mRNA and microRNA were quantified with the delta-delta Ct analysis, and the expression level of *ACTB* mRNA or snU6 small nuclear RNA was used for normalizing the mRNA or microRNA results respectively. The qPCR was performed as follows: 10 min at 95℃ for DNA polymerase activation and 50 cycles of 15 sec at 94℃, 20 sec at 57℃,

and 30 sec at 72℃. The identity and specificity of the amplified PCR product were validated by melting curve analysis. The sequences of the primers used in this study are described in Table 2.

Table 2. Primer sequences for qPCR

Primer	Sequence
ABCA1-F	AACAGTTTGTGGCCCTTTTG
ABCA1-R	AGTTCCAGGCTGGGGTACTT
ABCG1-F	ACGCAGTTCTGCATCCTCTT
ABCG1-R	CGGAGTTGCTCAAGACCTTC
ABCG5-F	CTCCTACAGCGTCAGCCAC
ABCG5-R	CGTTCACATACACCTCCCCC
ABCG8-F	GGACCTGACCAGCATTGACA
ABCG8-R	GCATCTTCGTAGGACTCGGG
HSPA5 (BiP)-F	CACTCCTGAAGGGGAACGTC
HSPA5 (BiP)-R	TCAACCACCTTGAACGGCAA
DERLIN 1-F	TTCTTGCACACATGCCTCTC
DERLIN 1-R	GCTGAGAAAACGCTTCATCC
Sel1L-F	AAGCCCTGGAGAGAGTGTCA
Sel1L-R	CCCCAAGAGCTCCAAATGTA
HERP-F	ACTTGCTTCCAAAGCAGGAA
HERP-R	CCCTTTGCCTTAAACCATCA
VCP-F	ATCCGTGAATCCATCGAGAG
VCP-R	GACTCTGCTGAAGGGTCTGG
MT1-F	GATCCTGGTTCTCCAGGTCA
MT1-R	CATTGAGGCAGCTGTTGAAA
MT2-F	CGGAACGCAGGTAATTTGTT
MT2-R	TAATGGCGATGGCAGTGATA
hsa-miR-7114-3p-F	GTGACCCACCCCTCTC
hsa-miR-195-5p-F	CGCAGTAGCAGCACAGA
hsa-miR-329-5p-F	GCAGGAGGTTTTCTGGGT
hsa-miR-338-5p-F	GCAGAACAATATCCTGGTGCT
hsa-miR-539-5p-F	GCAGGGAGAAATTATCCTTGGT
hsa-miR-545-3p-F	CGCAGTCAGCAAACATTTATTG
hsa-miR-548aj-3p-F	AGCGCAGTAAAAACTGCAA
hsa-miR-597-5p-F	GTGTCACTCGATGACCAC
hsa-miR-627-3p-F	CGCAGTCTTTTCTTTGAGACTC
hsa-miR-3130-5p-F	CCAGTCTCCGGTGCAG
hsa-miR-4650-3p-F	GCGCAGAGGTAGAATGAG
hsa-miR-6832-3p-F	CGCAGACCCTTTTTCTCT
hsa-miR-6845-3p-F	AGCCTCTCCTCCCTGT

hsa-miR-7854-3p-F	GTGAGGTGACCGCAGA
Universal reverse primer	Qiagen miScript Universal Primer

8. MicroRNA microarray

Starting with 250 ng of total RNA, labeling process begins with poly-A tailing of each RNA strand using poly A polymerase followed by ligation of biotin-labeled 3DNA dendrimer. Biotinylated RNA strands were hybridized at 48℃ for 18 h on Affymetrix GeneChip miRNA 4.0 Array (Affymetrix, Santa Clara, CA, US). The GeneChip miRNA 4.0 Array was washed and stained in the Affymetrix Fluidics Station 450. Amplified fluorescence signals by the branched structure of 3DNA dendrimer were scanned using Affymetrix GeneChip Scanner 3000 7G. The arrays were analyzed using an Affymetrix GeneChip scanner with associated software. miRNAs expression levels were calculated with Transcriptome Analysis Console Relative signal intensities for each miRNA were generated using the Robust Multi Array Average algorithm. The microarray data were analyzed with row z-score (Cheadle et al., 2003).

9. Annexin V-FITC/ PI staining

Fluorescein isothiocyanate-conjugated Annexin V (AnnexinV-FITC) and propidium iodide (PI) staining analysis was performed with an Annexin V-FITC apoptosis detection kit (BD Bioscience, Franklin Lakes, NJ, USA, #556547). After the experimental treatment, UCB-MSCs (1×10^5 cells) were detached from the dishes and collected cells were suspended in binding buffer. Annexin V-FITC and PI were added to the samples and incubated for 15 min at RT. Apoptosis of the samples was measured and analyzed with flow cytometry (CytoFlex; Beckman Coulter, Fullerton, CA, USA). Annexin V-FITC-positive and PI-positive (Q2), and Annexin V-FITC-positive and PI-negative (Q4) UCB-MSCs were considered

as late apoptotic, early apoptotic, respectively while Annexin V-FITC-negative and PI-positive (Q1) as necrosis. Annexin V-FITC-negative and PI-negative (Q3) UCB-MSCs were considered as viable. The following formula was used to determine the percentage of apoptotic cells: Apoptotic cells (%) = Q2 + Q4.

10. Water-soluble tetrazolium salt (WST-1) cell viability assay

The viabilities of the UCB-MSCs were measured by the WST-1 cell viability assay kit (EZCytox™; Daeil Lab service, Seoul, Korea, #EZ-1000). UCB-MSCs were cultured in 96-well plates and pretreated with DIDS or melatonin prior to cholesterol treatment for 24 h. After PBS washing, cells were incubated in 10% of EZ-Cytox™ solution in 100 μL of medium at 37℃ for 30 min. Then, the absorbance was measured with a microplate spectrophotometer (Epoch 2™, BioTek) at 450 nm.

11. Trypan blue exclusion assay

The UCB-MSCs were washed with PBS and detached by 0.05% trypsin solution incubation at 37℃ for 3 min. 10% FBS in PBS was added to the cell suspension to inhibit trypsin and spun down at 3,000 rpm speed to collect the cell. The cell pellet was suspended with 0.4% trypan blue (Sigma□Aldrich, #T6146) in PBS to stain the dead cells. Trypan blue-stained and -unstained cells were counted by using a Countess Ⅱ FL Automated Cell Counter (Thermo Fisher).

12. Measurements of intracellular ROS

To measure the intracellular ROS level, CM-H_2DCFDA (Thermo Fisher, #C6821) was used. After experimental treatment, the cells were washed with PBS and incubated in 1 mM of CM-H_2DCFDA in culture media at 37℃ for 30 min. The fluorescence intensity of CM-H_2DCFDA was measured with a luminometer (Victor3; PerkinElmer Inc., Waltham, MA, USA) at an excitation and emission wavelength of 485 and 535 nm.

13. Mouse skin wound healing model

All procedures for high-fat diet (HFD)-induced obese model and mouse skin wound healing model were performed following the National Institutes of Health Guidelines for Humane Treatment of Animals and approved by the Institutional Animal Care and Use Committee of Seoul National University (SNU-180802-2). To prepare obese mice model, HFD (Rodent Diet with 60 kcal% fat and 90 g added NaCl/4057 kcal, Research Diets Inc., New Brunswick, NJ, USA) was provided to 6-week old male institute of cancer research mice for 14 weeks. All mice were anesthetized with a mixture of Alfaxan™ (80 mg/kg, Jurox Pty Ltd, Rutheford, Australia) and xylazine HCl (10 mg/kg, Rompun™, Bayer, Leverkusen, Germany). The back of anesthetized mice was shaved and scrubbed with an organic iodine solution and 70% ethanol solution for disinfection during the surgery. The authors who have a doctor of veterinary medicine license granted by the Ministry of Agriculture and Forestry of the Republic of Korea performed wound surgery. A wound in the back skin was made by using a 6 mm diameter circular biopsy punch. UCB-MSCs were prepared with DIDS pretreatment for 24 h. Then,

1×10^6 UCB-MSCs were injected into the intradermally at three sites around each wound. After the surgery, wounds were covered with Tegaderm™ (3M, London, Canada). Experimental mice groups were divided into the 8 groups: normal diet (ND) feeding mice with injection of vehicle; ND feeding mice with injection of UCB-MSC; HFD feeding mice with injection of vehicle; HFD feeding mice with UCB-MSCs injection; HFD feeding mice with injection of UCB-MSCs and melatonin; HFD feeding mice with injection of melatonin; HFD feeding mice with injection of DIDS-pretreated UCB-MSCs and melatonin; HFD feeding mice with injection of DIDS-pretreated UCB-MSCs. Intraperitoneal injection of melatonin was conducted to the melatonin injection groups (30 mg/kg/day) for 12 days after wound formation. All gross images were acquired at post-injection days 0, 4, 8 and 12. The wound closure rate was analyzed by the ImageJ software. All mice were sacrificed at post-injection day 12. The Serum was separated from blood samples and the level of total cholesterol was measured by serum biochemistry instrument (Hitachi 7180 analyzer, Hitachi, Tokyo, Japan). For evaluating vasculogenesis, images of inner side of wound sites were obtained and analyzed with the Fiji software. Acquired skin samples were fixed with 4% paraformaldehyde (PFA) and then dehydrated with 20% and 30% sucrose solution. Dehydrated skin samples were embedded in optimum cutting temperature compound (Sakura Finetek, CA, USA, #4583) and stored in a deep freezer kept at □80℃. Frozen skin samples were sectioned to a 20 μm thickness using a cryostat (Leica CM 1520, Leica, Wetzlar, Germany) and mounted on silane-coated slides (Muto Pure Chemicals, Tokyo, Japan, #5116-20F).

14. Hematoxylin and eosin (H&E) staining

The tissue of skin wound was mounted on slides and fixed with 4% PFA for 5 min, and then stained with H&E for 5 min. Samples were washed with 70%, 95%, and 100% ethanol three times and then incubated in xylene for 5 min. All images were acquired by Eclipse Ts2™ fluorescence microscopy (Nikon, Tokyo, Japan). Histological evaluation and reepithelization scoring were performed in a blind fashion.

15. Masson's trichrome staining

The Masson's trichrome staining was performed according to the manufacture's protocol (Vitrovivo biotech, MD, USA, #VB3016). The frozen sectioned skin samples were fixed in 10% formalin for 30 min and rinsed in distilled water (DW) 3 times for 3 min. The samples were mordanted in Bouin's solution 60℃ for 1 h and washed in running tap water for 5 min. The samples were stained with Weigert's working hematoxylin for 7 min and blued in running tap water for 5 min. The samples were treated with Biebrich Scarlet-acid fuchsin solution for 5 min and washed in DW. After incubation of Phosphotungstic/phosphomolybdic acid solution for 10 min, the slides were transferred directly into Aniline blue solution for 5 min and rinsed in distilled water. The samples were treated with 1% Acetic acid for 1 min and dehydrated with 2 changes of 95% Ethanol and 100% Ethanol (2 min per change). After clearing with 3 changes of xylene (5 min per change), the slides were coverslipped with Ecomount (Biocare medical, CA, USA, #EM897L). All images were acquired by Eclipse Ts2™ fluorescence microscopy.

16. Immunohistochemistry

Skin samples on slides were fixed in 80% acetone solution for 20 min. Slides were washed in PBS and incubated in 5% NGS for 30 min. Samples were incubated with primary antibody in PBS containing 0.2% Tween-20 (PBST) for 2 h. After washing with PBST, samples were incubated with Alexa Fluor™ 488 or 555-conjugated secondary antibodies in PBST (1:100 dilution) for 1 h. All images were acquired by Eclipse Ts2™ fluorescence microscopy and analyzed with the Fiji software.

17. Statistical analysis

Statistical analysis and graphing were performed using statistics software, GraphPad Prism version 6.0 (GraphPad Inc., San Diego, CA, USA). Quantitative data are shown as the mean ± standard error of the mean. Comparing the means of treatment groups with that of the control was conducted with the Student's t-test and differences among more than three experimental groups were analyzed using one-way analysis of variance (ANOVA) with Dunnett's multiple comparison test. The $p < 0.05$ was considered statistically significant.

RESULTS

1. Effect of melatonin on ABCA1-induced cholesterol efflux in the presence of high cholesterol concentrations

When I measured apoptosis of UCB-MSCs treated with different concentrations of cholesterol (0□200 μM), I found that 200 μM cholesterol significantly reduced the survival of UCB-MSCs after 24 h (Fig. 1A and 1B). Cholesterol efflux depends on a membrane transporter, and I, therefore, determined the changes in the expression of genes encoding the cholesterol transporters *ABCA1, ABCG1, ABCG5, and ABCG8* (Schmitz et al., 2001). The level of the *ABCA1* mRNA was significantly increased in UCB-MSCs (Fig. 2A). Western blot results showed that the level of ABCA1 increased as well (Fig. 2B). The ABCA1 inhibitor DIDS (10 μM) was used to determine the role of ABCA1 in the regulation of intracellular cholesterol levels. DIDS treatment followed by the addition of cholesterol significantly increased the levels of intracellular cholesterol compared with cholesterol treatment alone (Fig. 2C). The western blot results showed that treating the cells with melatonin and cholesterol further increased ABCA1 expression compared with cholesterol treatment alone (Fig. 3A). To decipher the relationship between melatonin-induced ABCA1 expression and the regulation of intracellular cholesterol levels, cells were pretreated with DIDS or melatonin prior to cholesterol treatment, and the level of intracellular

cholesterol was measured. High concentrations of cholesterol added to the cultures increased the intracellular cholesterol levels, which were decreased when the cells were pretreated with melatonin. However, combined treatment with melatonin and DIDS did not cause a significant difference in increased cholesterol levels when cells were pretreated DIDS. These results indicate that ABCA1 is required to regulate the effect of melatonin on intracellular cholesterol levels (Fig. 3B). To verify the effect of melatonin on cholesterol efflux, I checked that the cholesterol concentration was increased in conditioned media. Cholesterol quantification results showed that melatonin treatment did not significantly change the cholesterol level of the media but decreased the intracellular cholesterol level (Fig. 3C). Taken together, the levels of ABCA1 were increased when cells were treated with high concentrations of cholesterol, and melatonin increased ABCA1 levels and cholesterol efflux.

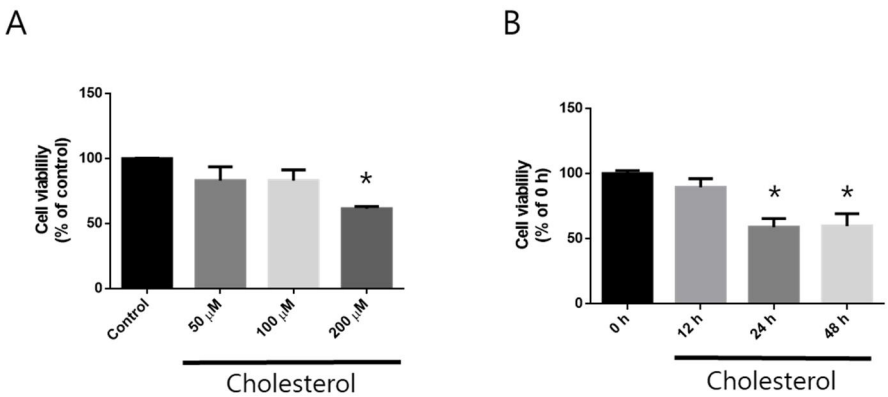

Figure 1. Effects of cholesterol treatment on the viability of UCB-MSCs. (A) UCB-MSCs were treated with various concentrations (0-200 μM) of cholesterol and then viability was measured by trypan blue exclusion assay (n=5, One-way ANOVA, $*p < 0.05$ vs control). (B) UCB-MSCs were treated with 200 μM of cholesterol for various times (0-48 h) and then viability was measured by trypan blue exclusion assay (n=5, One-way ANOVA, $*p < 0.05$ vs 0 h). All quantitative data are presented as a mean ± standard error of the mean.

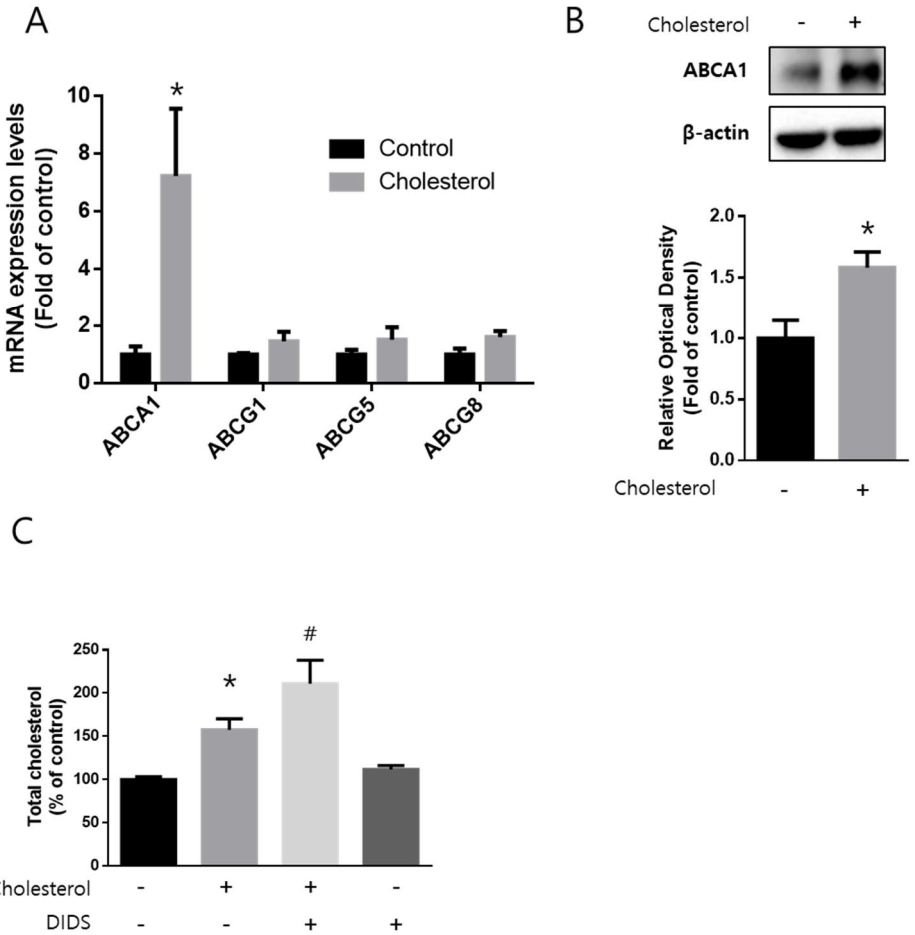
A
mRNA expression levels
(Fold of control)
10
8
6
4
2
0
*
Control
Cholesterol
ABCA1
ABCG1
ABCG5
ABCG8
B
Cholesterol - +
ABCA1
β-actin
Relative Optical Density
(Fold of control)
2.0
1.5
1.0
0.5
0.0
*
Cholesterol - +
C
Total cholesterol
(% of control)
250
200
150
100
50
0
*
#
Cholesterol - + + -
DIDS - - + +

Figure 2. The expression levels of cholesterol transporter under cholesterol condition and the role of ABCA1 on cholesterol efflux. UCB-MSCs were treated with 200 μM cholesterol for 24 h. (A) The expression levels of cholesterol transporter genes (*ABCA1, ABCG1, ABCG5, and ABCG8*) were measured by qPCR (n=5, Student's t-test, $*p < 0.05$ vs control). (B) The expression level of ABCA1 was quantified by western blot assay and relative optical density was measured by ImageJ (n=5, Student's t-test, $*p < 0.05$ vs control). (C) UCB-MSCs were pretreated with DIDS (10 μM) for 30 min prior to cholesterol treatment (200 μM, 24 h) and cellular cholesterol level was measured by cholesterol quantification kit (n=5, One-way ANOVA, $*p < 0.05$ vs control, $\#p < 0.05$ vs cholesterol). All blot images are representative and quantitative data are presented as a mean ± standard error of the mean.

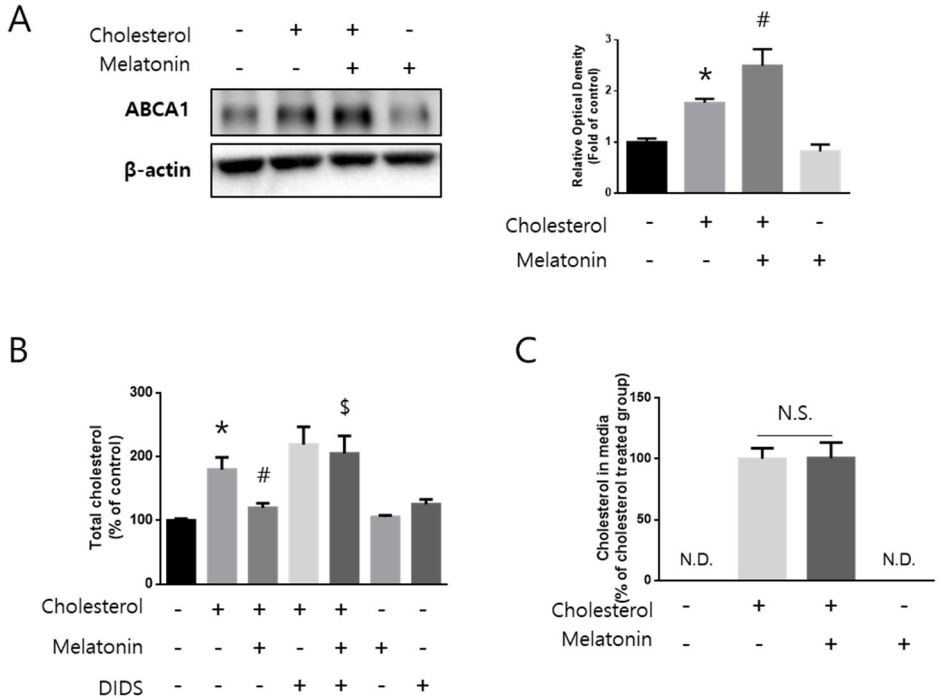

Figure 3. Effects of melatonin on ABCA1 expression and intracellular cholesterol level under high cholesterol condition. (A) Melatonin (1 μM) was pretreated for 30 min before cholesterol treatment (200 μM, 24 h) and the expression level of ABCA1 was measured by western blotting (n=5, One-way ANOVA, $*p < 0.05$ vs control, $\#p < 0.05$ vs cholesterol). (B) UCB-MSCs were pretreated with DIDS (10 μM) or melatonin (1 μM) for 30 min prior to cholesterol treatment and their total cholesterol levels were measured by quantification kit (n=5, One-way ANOVA, $*p < 0.05$ vs control, $\#p < 0.05$ vs cholesterol, $\$p < 0.05$ vs melatonin + cholesterol). (C) Melatonin (1 μM) was pretreated for 30 min before cholesterol treatment (200 μM, 24 h) and total cholesterol levels of cholesterol-conditioned media were measured by quantification kit. N.D. means not detected while N.S. means not significant. All blot images are representative and quantitative data are presented as a mean ± standard error of the mean.

2. Effects of melatonin on high cholesterol-induced intracellular ROS levels and apoptosis

To evaluate the association between high cholesterol levels and apoptosis, cholesterol-induced ROS was measured. Cholesterol treatment significantly increased ROS levels, which were further increased when cells were pretreated with DIDS (Fig. 4A). The effects of cholesterol on apoptotic cell death were assessed using western blotting and Annexin V/PI assays. The expressions of caspase 9, and caspase 3 and the percentages of apoptotic cell death were significantly increased by cholesterol, and DIDS treatment further increased the apoptosis of cholesterol-treated cells (Fig. 4B, and 4C). To determine the effect of melatonin on cholesterol-induced ROS levels and the involvement of ABCA1-dependent regulation of cholesterol efflux, cells were treated with cholesterol combined with DIDS or melatonin. Melatonin significantly decreased cholesterol-induced ROS, and combined treatment with DIDS and melatonin did not significantly change ROS levels compared with cells pretreated with DIDS (Fig. 5A). Western blot analysis revealed that melatonin decreased cholesterol-induced expressions of caspase 9 and caspase 3 (Fig. 5B). WST-1 assays of cell viability showed that melatonin restored the viability of cholesterol-treated cells to the control level, and there was no significant difference between treatment with DIDS before cells were exposed to cholesterol and cholesterol treatment of cells with DIDS and melatonin combined (Fig. 5C). Thus, melatonin alleviated the effects of cholesterol-induced ROS and apoptosis through cholesterol efflux mediated by increased expression of ABCA1.

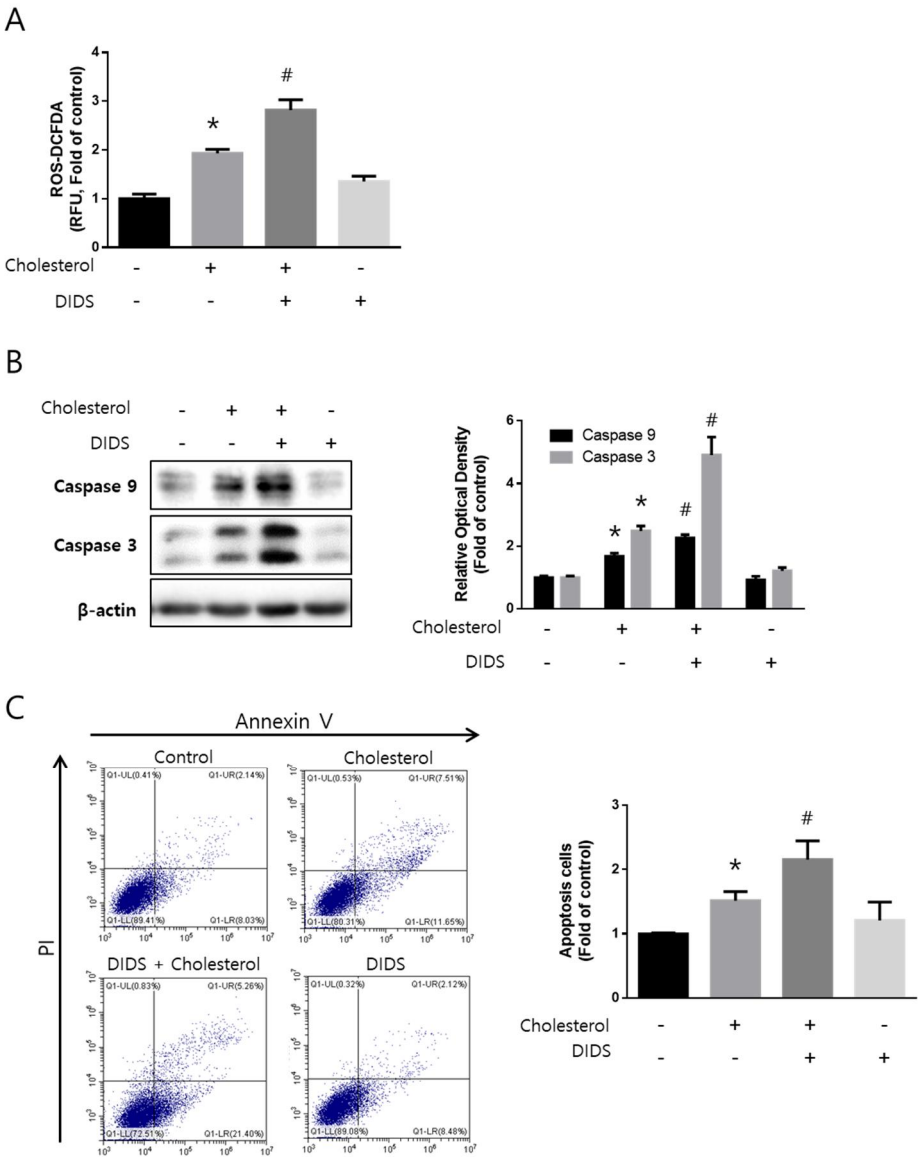
A
ROS-DCFDA
(RFU, Fold of control)
Cholesterol
DIDS
B
Caspase 9
Caspase 3
β-actin
Relative Optical Density
(Fold of control)
C
Annexin V
PI
Control
Cholesterol
DIDS + Cholesterol
DIDS
Apoptosis cells
(Fold of control)

Figure 4. Roles of ABCA1 on cholesterol-induced ROS and apoptosis of UCB-MSCs. UCB-MSCs were pretreated with DIDS (10 μM) for 30min prior to cholesterol treatment (200 μM, 24 h). (A) The intracellular ROS level was measured by CM-H_2DCFDA. The relative fluorescence units (RFU) was measured by luminometer (n=5, One-way ANOVA, $*p < 0.05$ vs control, $\#p < 0.05$ vs cholesterol). (B) The expression level of caspase 9 and 3 were quantified by western blotting (n=5, One-way ANOVA, $*p < 0.05$ vs control, $\#p < 0.05$ vs cholesterol). (C) The percentage of apoptosis was analyzed with Annexin V/PI assay. Annexin V-FITC-positive and PI-positive (Q2), and Annexin V-FITC-positive and PI-negative (Q4) UCB-MSCs were considered as late apoptotic and early apoptotic, respectively (n=5, One-way ANOVA, $*p < 0.05$ vs control, $\#p < 0.05$ vs cholesterol). All images and are representative and quantitative data are presented as a mean ± standard error of the mean.

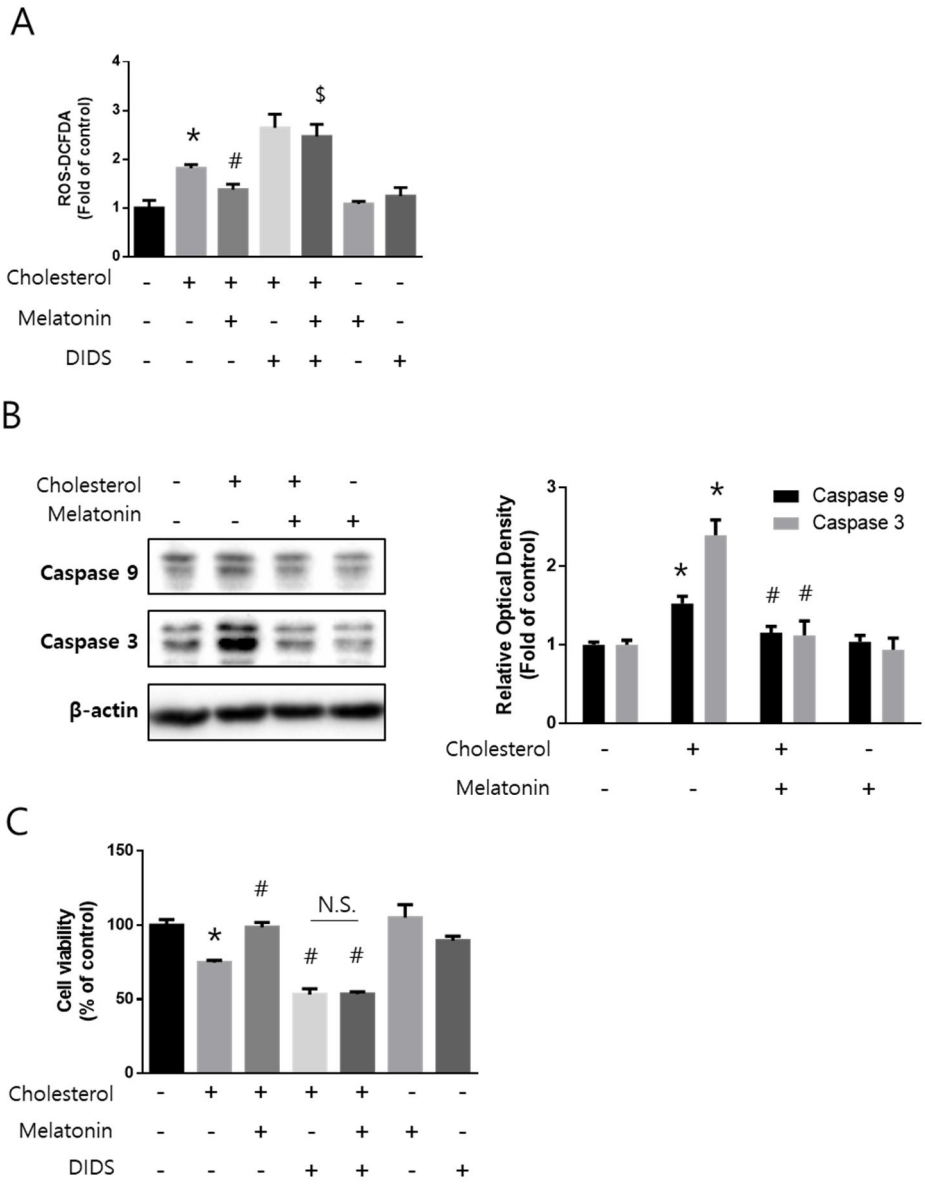
A
ROS-DCFDA
(Fold of control)
Cholesterol
Melatonin
DIDS
B
Cholesterol
Melatonin
Caspase 9
Caspase 3
β-actin
Relative Optical Density
(Fold of control)
Caspase 9
Caspase 3
C
Cell viability
(% of control)
N.S.

Figure 5. Effects of melatonin on high cholesterol-induced ROS accumulation and apoptosis. (A) UCB-MSCs were pretreated with melatonin (1 μM) or DIDS (10 μM) for 30 min prior to cholesterol treatment (200 μM, 24 h), and the level of total ROS was measured by CM-H_2DCFDA (n=5, One-way ANOVA, $*p < 0.05$ vs control, $\#p < 0.05$ vs cholesterol, $\$p < 0.05$ vs melatonin + cholesterol). (B) UCB-MSCs were pretreated with melatonin (1 μM) for 30min prior to cholesterol treatment (200 μM, 24 h) and then the expression levels of caspase 9 and 3 were measured by western blotting (n=5, One-way ANOVA, $*p < 0.05$ vs control, $\#p < 0.05$ vs cholesterol). (C) The cells were pretreated with melatonin (1 μM) or DIDS (10 μM) for 30 min prior to cholesterol treatment (200 μM, 24 h), and cell viability was measured with WST-1 assay (n=5, One-way ANOVA, $*p < 0.05$ vs control, $\#p < 0.05$ vs cholesterol, n.s. means not significant). All blot images are representative and quantitative data are presented as a mean $\pm$ standard error of the mean.

3. Effect of melatonin on the therapeutic efficacy of transplanted UCB-MSCs in a mouse model of HFD-induced obesity

To identify the effect of melatonin on UCB-MSCs transplanted into skin wounds, mice were induced to become obese by feeding them a HFD for 14 weeks. The mice exhibited higher weight and total cholesterol levels than mice fed a ND (Fig. 6A and 6B). To determine the difference between the efficacy of UCB-MSC transplantation of obese and normal mice, skin-injury recovery model was used. On day 12, after causing the skin injury, the transplantation efficacies were compared by measuring the sizes of wound closures. The wound sizes of UCB-MSC-transplanted HFD mice were significantly larger than that of UCB-MSC-transplanted ND mice. Melatonin restored the wound sizes of UCB-MSC-transplanted HFD mice to those of the UCB-MSC-transplanted ND mice. However, in mice transplanted with DIDS-pretreated UCB-MSC cells, melatonin did not exhibit the recovery effect of melatonin (Fig. 7). In addition, we compared the vasculogenesis around the wound sites and the results showed that the effect of UCB-MSCs on vasculogenensis was recovered by melatonin treatment which was lowered in HFD mice (Fig. 8). To verify the antiapoptotic effect of melatonin on the engrafted UCB-MSCs, their survival rate was measured, indicated by the expression of human nuclear antigen in the wounded tissues of UCB-MSC transplanted mice. Melatonin-treated HFD mice harbored the same number of UCB-MSCs as transplanted ND mice, which decreased when the cells were pretreated with DIDS (Fig. 9). Histological scores for re-epithelialization indicated that melatonin treatment increased the extent of re-epithelialization of UCB-MSC-

transplanted mice compared with other HFD mice (Fig. 10A). In addition, fibrosis was measured to evaluate the efficacy of wound healing therapy with Masson's trichrome staining and immunohistochemistry using alpha-smooth muscle antigen (α-SMA) antibody. (Gupta et al., 2017; Parfejevs et al., 2018) The results showed that fibrosis in granulation tissue increased with melatonin treatment, whereas inhibition of ABCA1 of UCB-MSCs diminished these effects (Fig. 10B and 10C). Thus, the efficacy of MSC transplantation for treating obese condition was improved by the ABCA1-dependent effects of melatonin.

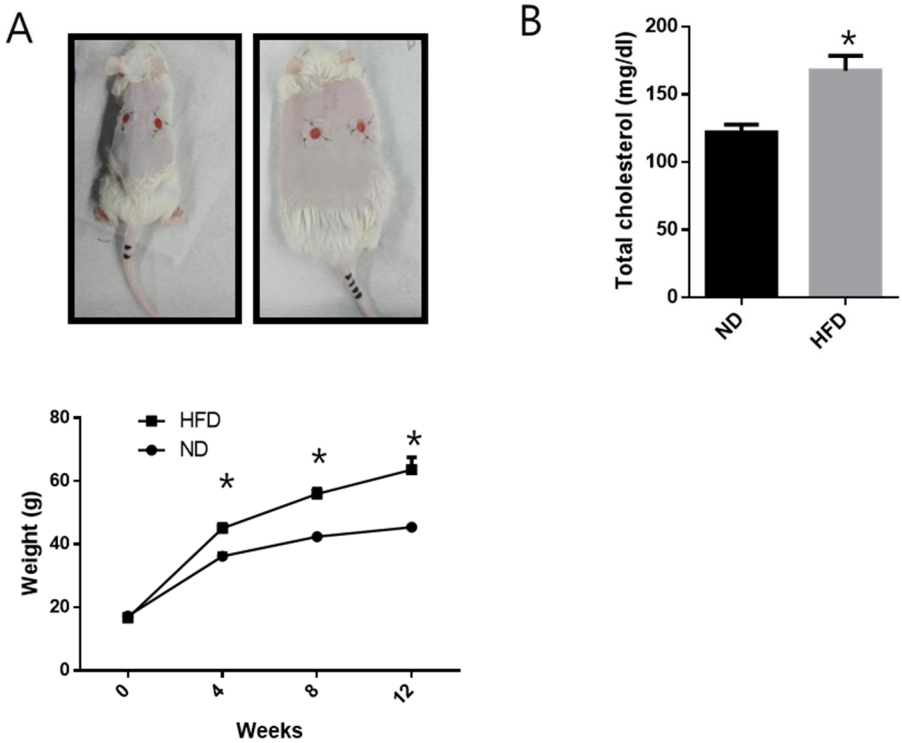

Figure 6. High-fat-diet-induced obese mouse model. Obese mouse model was prepared by feeding high-fat-diet (HFD) for 14 weeks. (A) Weights of HFD-induced obese mice were compared with normal diet (ND) feeding mice (n=7, Student's t-test, $*p < 0.05$ vs ND). (B) The levels of total cholesterol in serum of HFD-induced obese mice were compared with ND feeding mice (n=7, Student's t-test, $*p < 0.05$ vs ND). All images are representative and quantitative data are presented as a mean ± standard error of the mean.

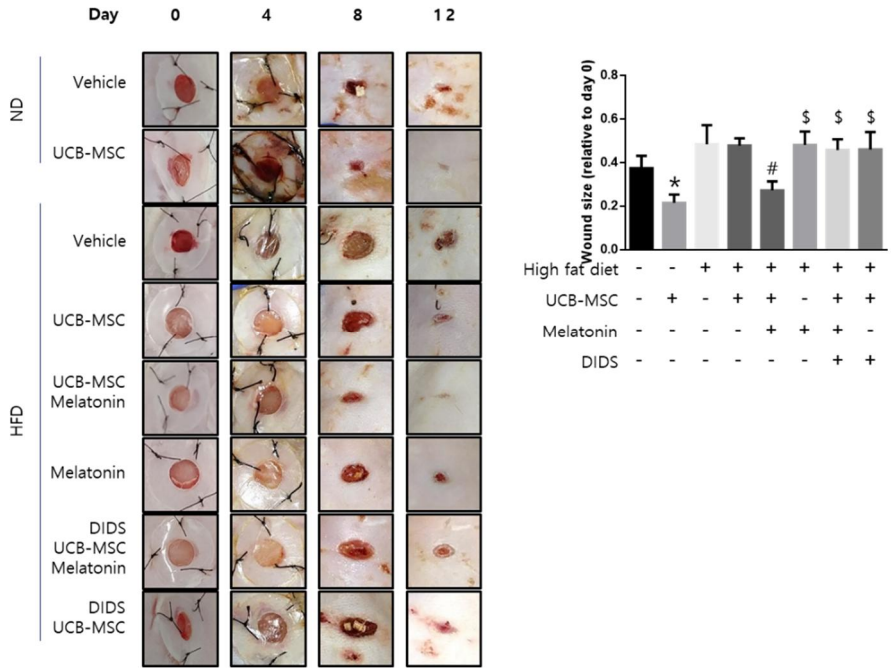

Figure 7. Effects of melatonin on wound closure in the HFD-induced obese mouse model. Mice were divided into the 8 groups and skin wound healing model was conducted: ND + vehicle; ND + UCB-MSC; HFD + vehicle; HFD + UCB-MSC; HFD + UCB-MSC + melatonin; HFD + melatonin; HFD + DIDS-pretreated UCB-MSC + melatonin; HFD + DIDS-pretreated UCB-MSC. After making wounds on the skin of the back, UCB-MSCs with or without DIDS pretreatment were inoculated near the wound site and melatonin (30 mg/kg/day) was injected to the mice of melatonin treatment group. Wounds on skin was observed on every 4 days and their size was compared (n=7, One-way ANOVA, $*p < 0.05$ vs ND + vehicle, $\#p < 0.05$ vs HFD + UCB-MSC, $\$p < 0.05$ vs HFD + UCB-MSC + Melatonin). All images are representative and quantitative data are presented as a mean ± standard error of the mean.

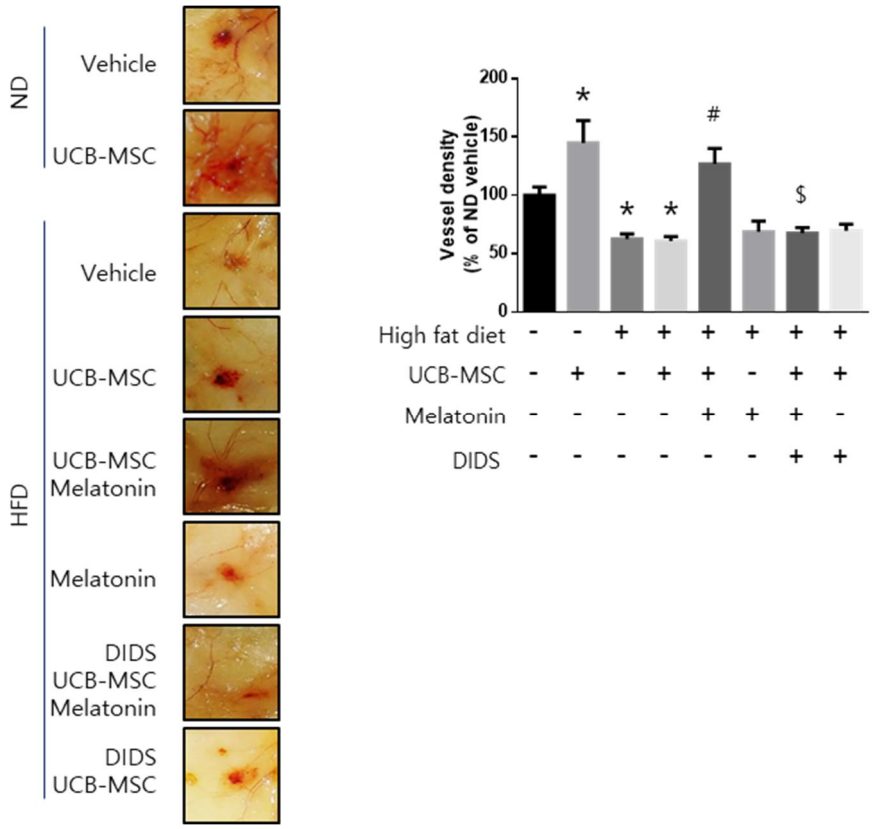

Figure 8. Effects of melatonin on vasculogenesis in the HFD-induced obese mouse model. Mice were divided into the 8 groups and skin wound healing model was conducted. After making wounds on the skin of the back, UCB-MSCs with or without DIDS pretreatment were inoculated near the wound site and melatonin (30 mg/kg/day) was injected to the mice of melatonin treatment group. vasculogenesis around the wound site was compared using vessel density analyze software (n=5, One-way ANOVA, $*p < 0.05$ vs ND + UCB-MSC, $\#p < 0.05$ vs HFD + UCB-MSC, $\$p < 0.05$ vs HFD + UCB-MSC + Melatonin). All images are representative and quantitative data are presented as a mean ± standard error of the mean.

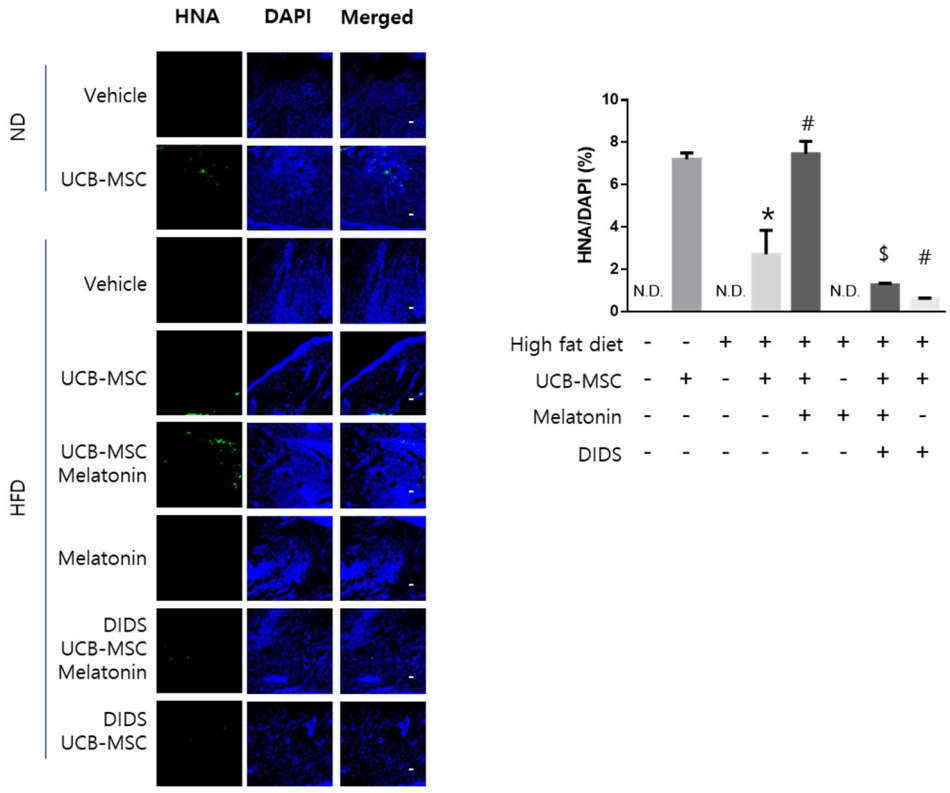

Figure 9. Effects of melatonin on the survival rate of transplanted UCB-MSCs in the HFD-induced obese mouse model. Mice were divided into the 8 groups and skin wound healing model was conducted. Immunohistochemistry was conducted with an antibody for human nuclear antigen (HNA, green) and DAPI (blue) staining and visualized by fluorescence microscopy. Scale bars were set as 100 μm (magnification $\times$100). The percentage of HNA-positive cells in total cells were analyzed with Fiji software (n=5, One-way ANOVA, *$p < 0.05$ vs ND + UCB-MSC, #$p < 0.05$ vs HFD + UCB-MSC, \$$p < 0.05$ vs HFD + UCB-MSC + Melatonin, N.D. indicates not detected). All images are representative and quantitative data are presented as a mean $\pm$ standard error of the mean.

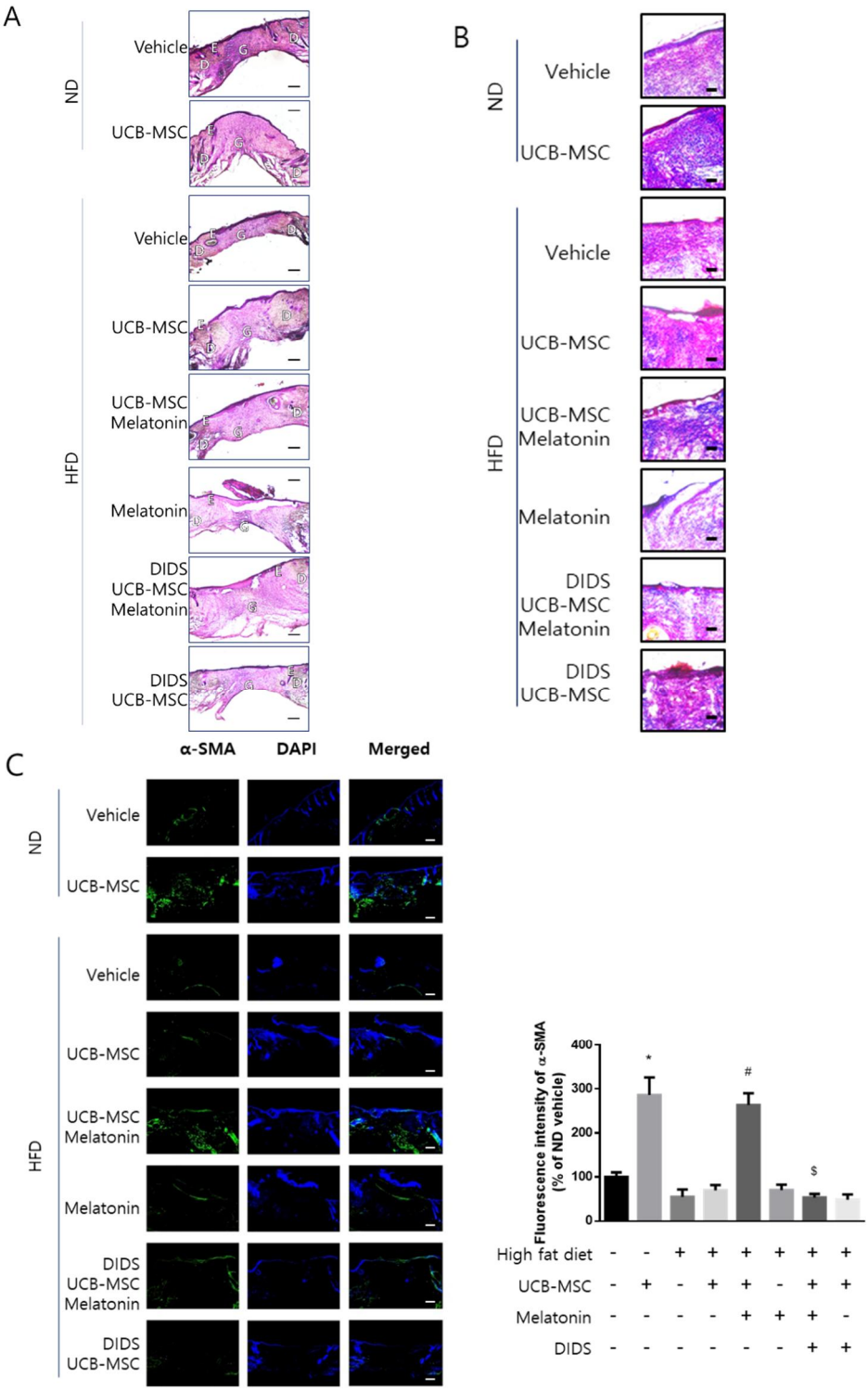
A
ND
Vehicle
UCB-MSC
HFD
Vehicle
UCB-MSC
UCB-MSC
Melatonin
Melatonin
DIDS
UCB-MSC
Melatonin
DIDS
UCB-MSC
B
ND
Vehicle
UCB-MSC
HFD
Vehicle
UCB-MSC
UCB-MSC
Melatonin
Melatonin
DIDS
UCB-MSC
Melatonin
DIDS
UCB-MSC
C
α-SMA
DAPI
Merged
ND
Vehicle
UCB-MSC
HFD
Vehicle
UCB-MSC
UCB-MSC
Melatonin
Melatonin
DIDS
UCB-MSC
Melatonin
DIDS
UCB-MSC
Fluorescence intensity of α-SMA
(% of ND vehicle)
400
300
200
100
0
*
#
$
High fat diet - - + + + + + +
UCB-MSC - + - + + - + +
Melatonin - - - - + + + -
DIDS - - - - - - + +

Figure 10. Effects of melatonin on skin tissue regeneration in the HFD-induced obese mouse model. Mice were divided into the 8 groups and skin wound healing model was conducted. After making wounds on the skin of the back, UCB-MSCs with or without DIDS pretreatment were inoculated near the wound site and melatonin (30 mg/kg/day) was injected to the mice of melatonin treatment group. (A) Hematoxylin and eosin staining were conducted on tissues of wound site. Scale bars are 200 μm (magnification ×50). D dermis, E epidermis, G granulation tissue. (B) Masson's trichrome staining was conducted on skin wound tissues. Scale bars are 100 μm (magnification ×100). (C) Immunohistochemistry was conducted with an antibody for alpha-smooth muscle antigen (α-SMA, green) and DAPI (blue) staining and visualized by fluorescence microscopy. Scale bars were set as 200 μm (magnification ×50). The fluorescence intensity of α-SMA in granulation tissue was analyzed with Fiji software (n=5, One-way ANOVA, $*p < 0.05$ vs ND + UCB-MSC, $\#p < 0.05$ vs HFD + UCB-MSC, $\$p < 0.05$ vs HFD + UCB-MSC + Melatonin). All images are representative and quantitative data are presented as a mean ± standard error of the mean.

4.Role of MT2-dependent BiP/NRF1 inhibition of melatonin-induced ABCA1 expression

When I determined the levels of mRNAs and proteins of melatonin receptors 1A and 1B (*MTNR1A* and *MTNR1B*) using qPCR and western blotting, I found that the mRNA level of *MTNR1B* and expression level of MT2 was increased in cholesterol-treated UCB-MSCs (Fig. 11A and 11B). NRF1 regulates cholesterol homeostasis by repressing the activity of LXRα, which is a major transcription factor that drives the expression of ABCA1. Further, the nuclear translocation of NRF1 is regulated by ERAD (Choi et al., 2017; Fang et al., 2018; Widenmaier et al., 2017). Therefore, I determined the melatonin-dependent changes in the mRNA expression of the ERAD-related proteins *HSPA5* (BiP), *DERL1*, *HERPUD1*, *SEL1L*, and *VCP* under conditions of high cholesterol concentrations. The qPCR results showed that cholesterol treatment following melatonin treatment significantly decreased the levels of *HSPA5A* mRNA (Fig. 12A). The competitive MT2 antagonist 4-phenyl-2-propionamidotetralin (4-P-PDOT) was used to determine if the regulatory effect of melatonin on BiP was MT2-dependent. The western blot results showed that 4-P-PDOT treatment abolished the melatonin-induced decrease of BiP expression (Fig. 12B). To confirm these findings, immunocytochemistry was conducted. The data revealed that melatonin treatment further decreased the co-localization of BiP and NRF1 as well as the nuclear translocation of NRF1 compared with cholesterol-treated cells (Fig. 13A and 13B). To confirm the regulatory effect of NRF1 on ABCA1 expression and cholesterol efflux, I determined the effect of an *NRF1*-specific siRNA on the levels of ABCA1 and intracellular cholesterol levels in

the presence of high cholesterol concentrations. Under these conditions, knockdown of *NRF1* increased the levels of ABCA1 and decreased the intracellular cholesterol levels compared with those of cells transfected with the NT siRNA (Fig. 14A and 14B). Thus, melatonin increased ABCA1 expression via MT2-dependent inhibition of the BiP expression and the nuclear translocation of NRF1.

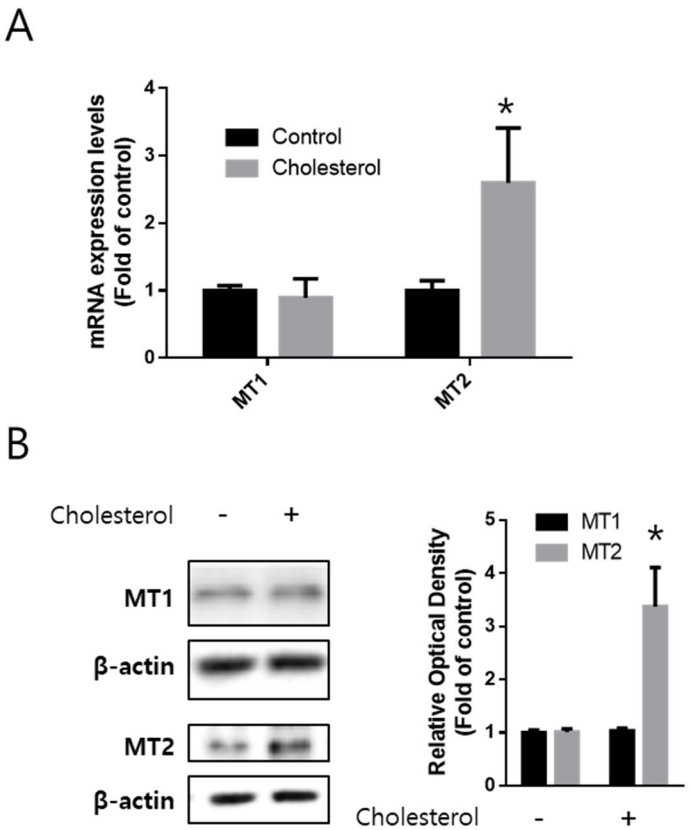

Figure 11. The expression levels of melatonin receptors under cholesterol condition. (A) Cholesterol (200 μM, 24 h) was treated to UCB-MSCs and the changes in mRNA expression levels of melatonin receptors were measured by qPCR (n=5, Student's t-test, $*p < 0.05$ vs control). (B) Cholesterol (200 μM, 24 h) was treated to UCB-MSCs and the changes in expression levels of melatonin receptors were measured by western blotting (n=5, Student's t-test, $*p < 0.05$ vs control). All blot and images are representative and quantitative data are presented as a mean ± standard error of the mean.

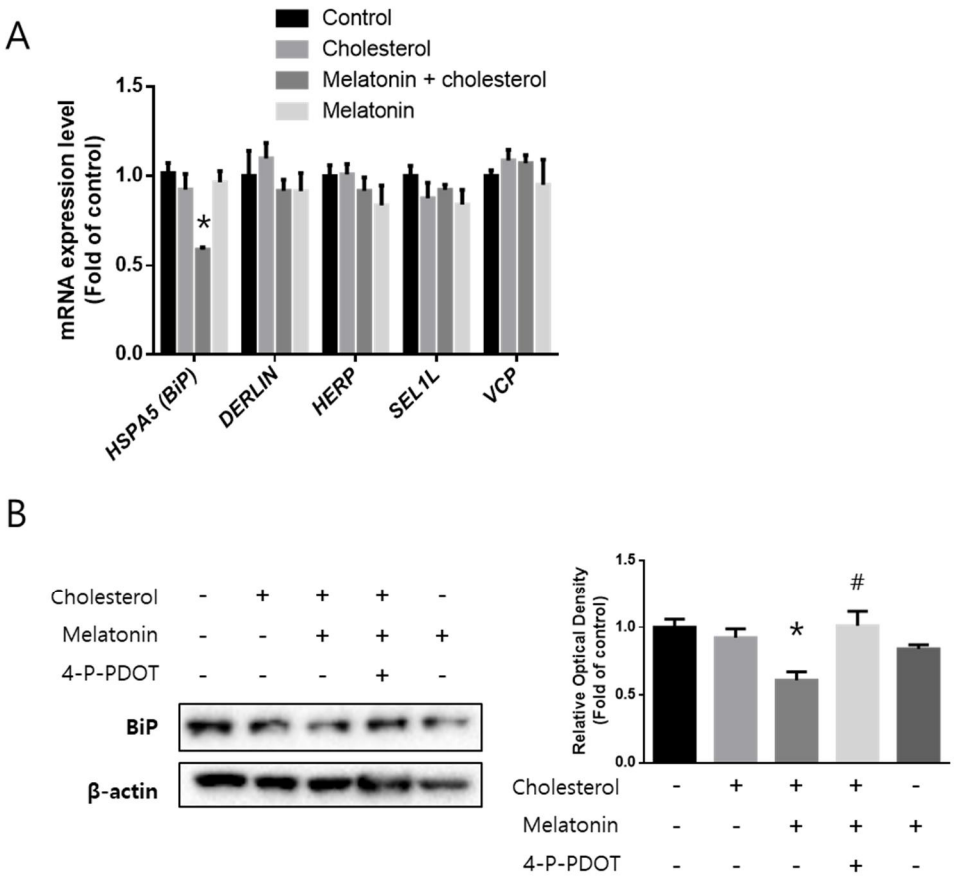

Figure 12. Effects of melatonin on ERAD-related genes and MT2-dependent suppression of BiP. (A) Melatonin (1 μM) was pretreated to UCB-MSCs for 30 min before cholesterol treatment (200 μM, 24 h) and then the expression levels of *HSPA5, DERLIN, HERP, SEL1L,* and *VCP* were compared (n=5, One-way ANOVA, $*p < 0.05$ vs control). (B) MT2 inhibitor, 4-P-PDOT (10 μM) were pretreated for 30 min prior to melatonin treatment (1 μM) and cholesterol (200 μM) and then the expression level of BiP was measured by western blotting (n=5, One-way ANOVA, $*p < 0.05$ vs control, $\#p < 0.05$ vs cholesterol + melatonin). All blot and images are representative and quantitative data are presented as a mean ± standard error of the mean.

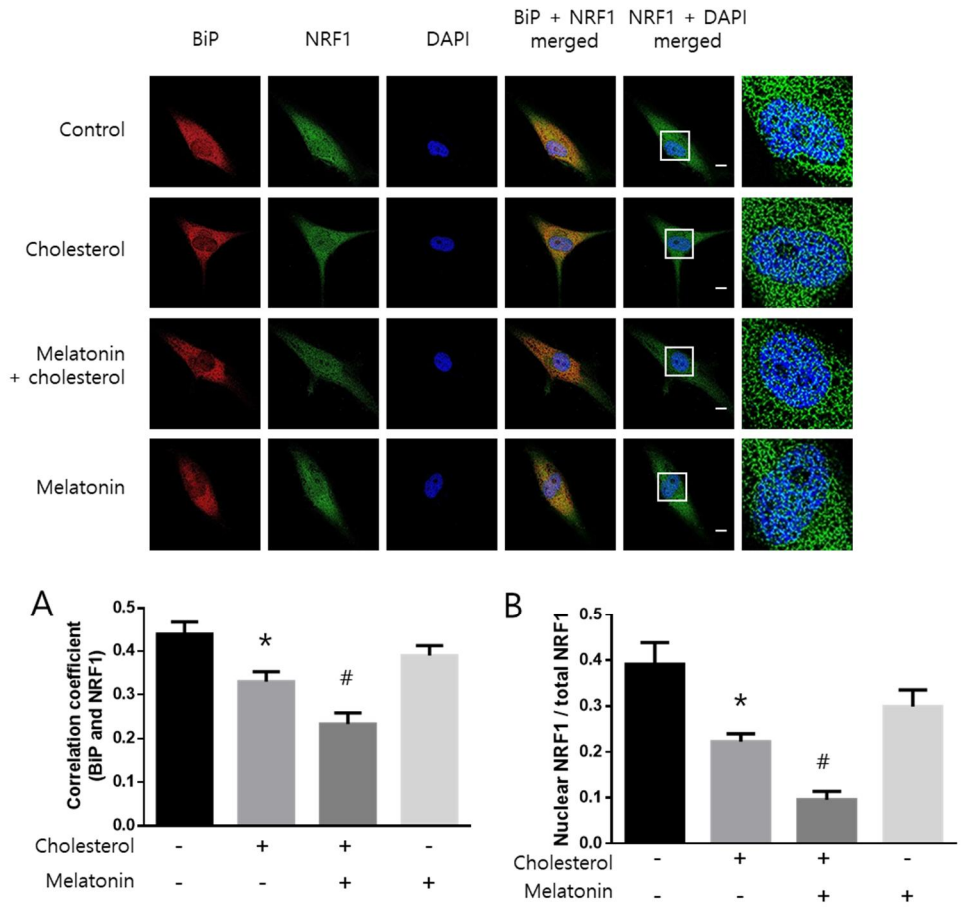

Figure 13. The role of melatonin on BiP-dependent nuclear translocation of NRF1. (A) Immunocytochemistry was conducted with NRF1 (green) and BiP (red) specific antibodies and DAPI (blue) and then visualized by SRRF imaging system. Scale bar was set as 8 μm (Magnification ×1,000). (A) The co-localization of NRF1 and Bip and nuclear translocation of NRF1 was analyzed with the correlation coefficient by Fiji software (n=5, One-way ANOVA, $*p < 0.05$ vs control, $\#p < 0.05$ vs cholesterol). (B) Nuclear translocation of NRF1 was analyzed by ratio of nuclear NRF1 to total NRF1 (n=5, One-way ANOVA, $*p < 0.05$ vs control, $\#p < 0.05$ vs cholesterol). All images are representative and quantitative data are presented as a mean ± standard error of the mean.

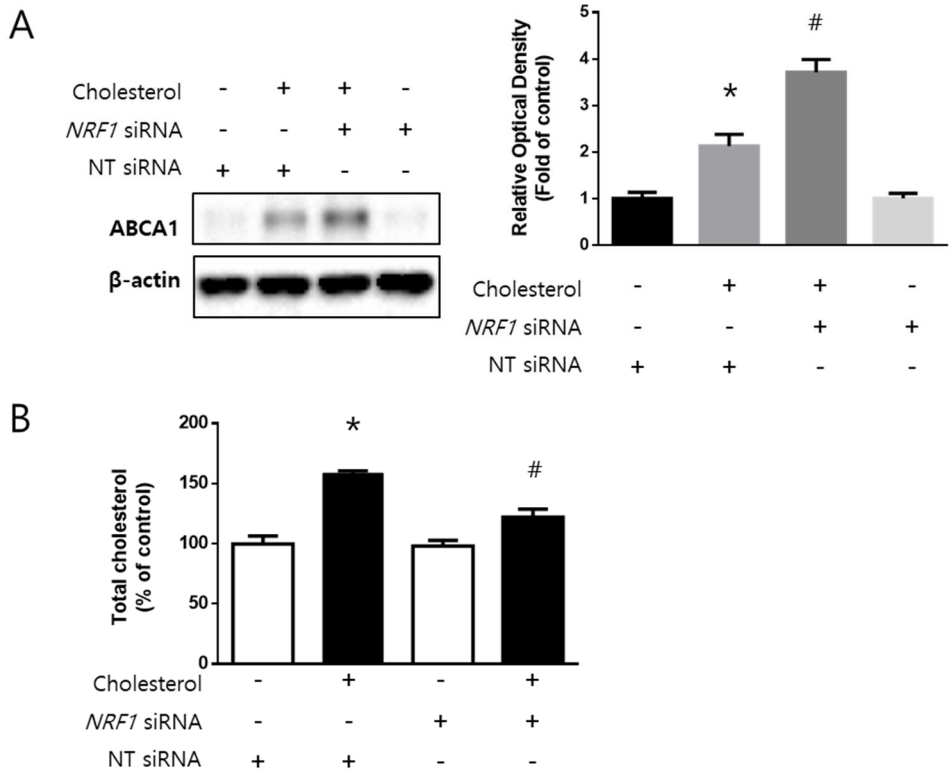

Figure 14. Role of NRF1 on ABCA1 expression and regulation of intracellular cholesterol level. *NRF1* or NT siRNA was transfected to UCB-MSCs for 24 h using transfection reagents prior to cholesterol treatment (200 μM, 24 h). (A) The changes of ABCA1 expression was measured by western blotting (n=5, One-way ANOVA, $*p < 0.05$ vs NT siRNA, $\#p < 0.05$ vs NT siRNA + cholesterol). (B) The level of total cholesterol was quantified with cholesterol quantification kit (n=5, One-way ANOVA, $*p < 0.05$ vs NT siRNA, $\#p < 0.05$ vs NT siRNA + cholesterol). All blot and images are representative and quantitative data are presented as a mean ± standard error of the mean.

5. Roles of BiP in the nuclear translocation of NRF1 and ABCA1 expression in the presence of high cholesterol concentrations

To assess the role of BiP in the ERAD-dependent nuclear translocation of NRF1, the cells were treated with the BiP inhibitor Ver155008 (10 μM) and immunocytochemistry was performed to detect co-localization of NRF1 and BiP as well as the nuclear translocation of NRF1. Ver155008 decreased the co-localization of NRF1 and BiP to a greater extent than that of cholesterol-treated cells, and the nuclear translocation of NRF1 similarly decreased (Fig. 15A and 15B). I determined whether decreased nuclear translocation of NRF1 caused by BiP affected the expression of ABCA1. The levels of ABCA1 in UCB-MSCs treated with Ver155008 and then with cholesterol increased more than those of cells treated with cholesterol alone (Fig. 16A). To assess the effect of BiP inhibition on NRF1-dependent regulation of the levels of intracellular cholesterol and ROS as well as on cholesterol-induced apoptosis, the levels of cholesterol and ROS were quantitated and Annexin V/PI analyses was used to measure apoptosis. The results that treating the cells with Ver155008 and then with cholesterol decreased intracellular cholesterol levels, ROS and apoptosis of UCB-MSCs in the presence of high cholesterol concentrations (Fig. 16B, 16C, and 16D). Collectively, I found that the suppression of BiP decreased the nuclear translocation of NRF1, which increased the levels of ABCA1 and decreased the levels of cholesterol as well as high-cholesterol-induced apoptosis.

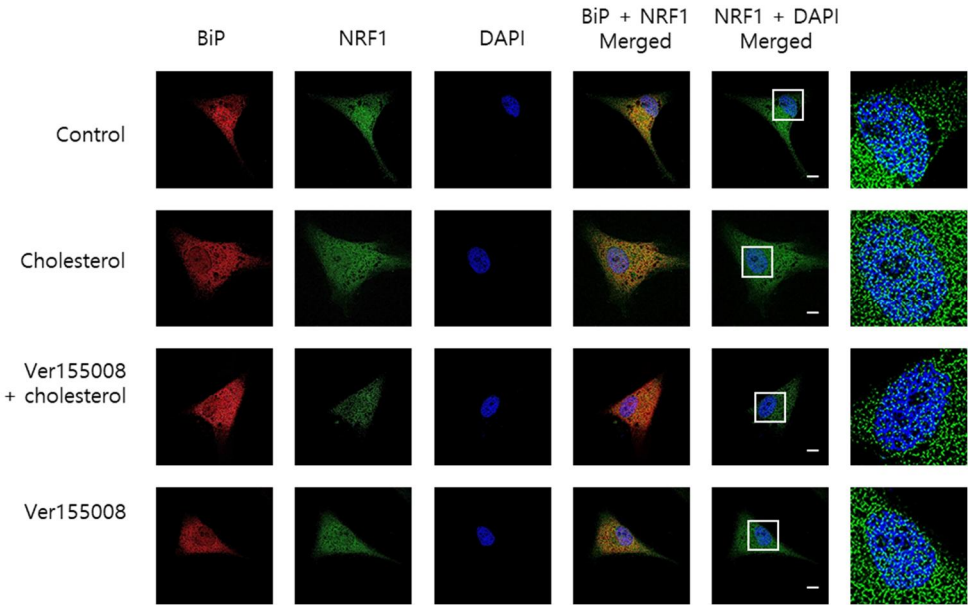
BiP
NRF1
DAPI
BiP + NRF1
Merged
NRF1 + DAPI
Merged
Control
Cholesterol
Ver155008
+ cholesterol
Ver155008

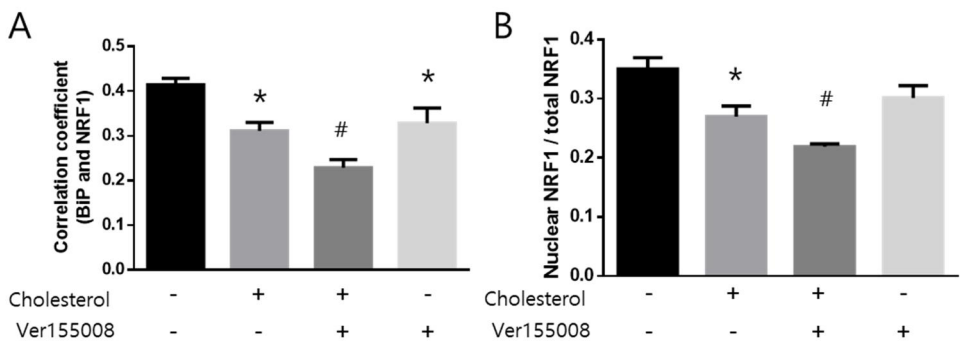
A
Correlation coefficient
(BiP and NRF1)
0.5
0.4
0.3
0.2
0.1
0.0
*
#
*
Cholesterol - + + -
Ver155008 - - + +
B
Nuclear NRF1 / total NRF1
0.4
0.3
0.2
0.1
0.0
*
#
Cholesterol - + + -
Ver155008 - - + +

Figure 15. Role of Bip on translocation of nuclear NRF1 under high cholesterol condition. UCB-MSCs were pretreated BiP inhibitor, Ver155008 (10 μM) for 30 min prior to cholesterol treatment (200 μM, 24 h). (A) Immunocytochemistry was conducted with NRF1 (green), BiP (red) specific antibodies and DAPI (blue), and then visualized by SRRF imaging system. Scale bar was set as 8 μm (Magnification ×1,000). (A) The co-localization of NRF1 and Bip and nuclear translocation of NRF1 was analyzed with the correlation coefficient by Fiji software (n=7, One-way ANOVA, $*p < 0.05$ vs control, $\#p < 0.05$ vs cholesterol). (B) Nuclear translocation of NRF1 was analyzed by ratio of nuclear NRF1 to total NRF1 (n=5, One-way ANOVA, $*p < 0.05$ vs control, $\#p < 0.05$ vs cholesterol). All images are representative and quantitative data are presented as a mean ± standard error of the mean.

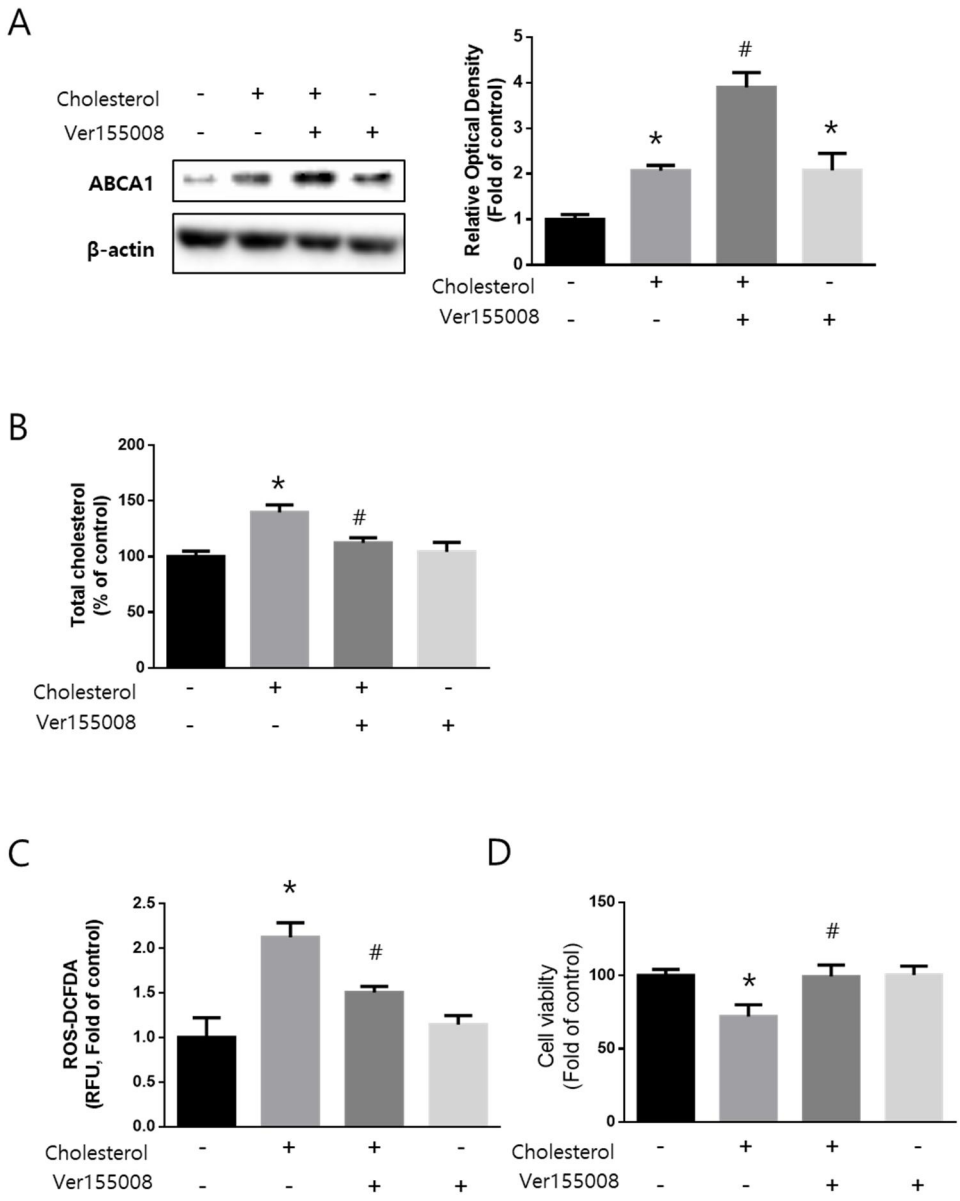
A
Cholesterol - + + -
Ver155008 - - + +
ABCA1
β-actin
Relative Optical Density (Fold of control)
B
Total cholesterol (% of control)
C
ROS-DCFDA (RFU, Fold of control)
D
Cell viability (Fold of control)

Figure 16. Role of Bip on ABCA1 expression, high-cholesterol-induced cholesterol accumulation and apoptosis. UCB-MSCs were pretreated BiP inhibitor, Ver155008 (10 μM) for 30 min prior to cholesterol treatment (200 μM, 24 h). (A) The expression level of ABCA1 was quantified with western blotting (n=5, One-way ANOVA, $*p < 0.05$ vs control, $\#p < 0.05$ vs cholesterol). (B) The concentration of the intracellular cholesterol was measured with cholesterol quantification kit (n=5, One-way ANOVA, $*p < 0.05$ vs control, $\#p < 0.05$ vs cholesterol). (C) Cells were incubated with CM-H_2DCFDA and relative fluorescence units (RFU) was measured by luminometer (n=5, One-way ANOVA, $*p < 0.05$ vs control, $\#p < 0.05$ vs cholesterol). (D) Cell viability was measured by trypan blue exclusion assay (n=5, One-way ANOVA, $*p < 0.05$ vs control, $\#p < 0.05$ vs cholesterol). All blots are representative and quantitative data are presented as a mean ± standard error of the mean.

6. Role of Sp1-induced miR-597 in the inhibition of expression of BiP by melatonin

Next, I investigated the regulation of BiP expression by melatonin through the MT2 signaling pathway. For this purpose, I determined if the expression of BiP was regulated by microRNA. 83 BiP-targeting microRNAs were selected from three databases (Genecards, microRNA.org, and Diana tools) and I conducted microRNA microarray to select the increased microRNA candidates with melatonin treatment. The microarray data were analyzed with row z-score with hierarchical clustering to compare the changes in expression levels of microRNAs and I found a cluster of 14 candidate microRNAs in which the expression levels were increased by melatonin treatment (Fig. 17A). To confirm the expression level of candidate microRNAs under cholesterol and melatonin conditions, qPCR was conducted and the results showed that miR-597-5p was significantly increased with melatonin treatment (Fig. 17B). miR-597 mimic was used to determine whether BiP expression was controlled by miR-597-5p. The qPCR and western blot results revealed that the miR-597-5p mimic suppressed BiP expression and upregulated ABCA1 expression compared with cholesterol-treated cells (Fig. 18A, and 18B). Among transcription factors that are regulated by MT2-dependent signaling pathways and candidates that bind the promoter region of miR-597, Sp1 was selected. First, I checked if the effect of melatonin on activation of Sp1 is MT2-dependent with 4-P-PDOT. Thr453 phosphorylation of Sp1, which activates Sp1, increased with melatonin treatment but decreased when cells were pretreated with 4-P-PDOT (Fig. 19A).

Immunocytochemistry revealed that nuclear translocation of Sp1 increased in response to melatonin, which was inhibited when cells were pretreated with 4-P-PDOT (Fig. 19B). Next, to verify the role of Sp1 in the regulation of miR-597 expression, cells were pretreated with Mithramycin A to inhibit the activation of Sp1. The results revealed that Mithramycin A decreased melatonin-induced miR-597 expression (Fig. 19C). Thus, melatonin decreased the expression of BiP through an MT2-Sp1-dependent miR-597 regulatory pathway.

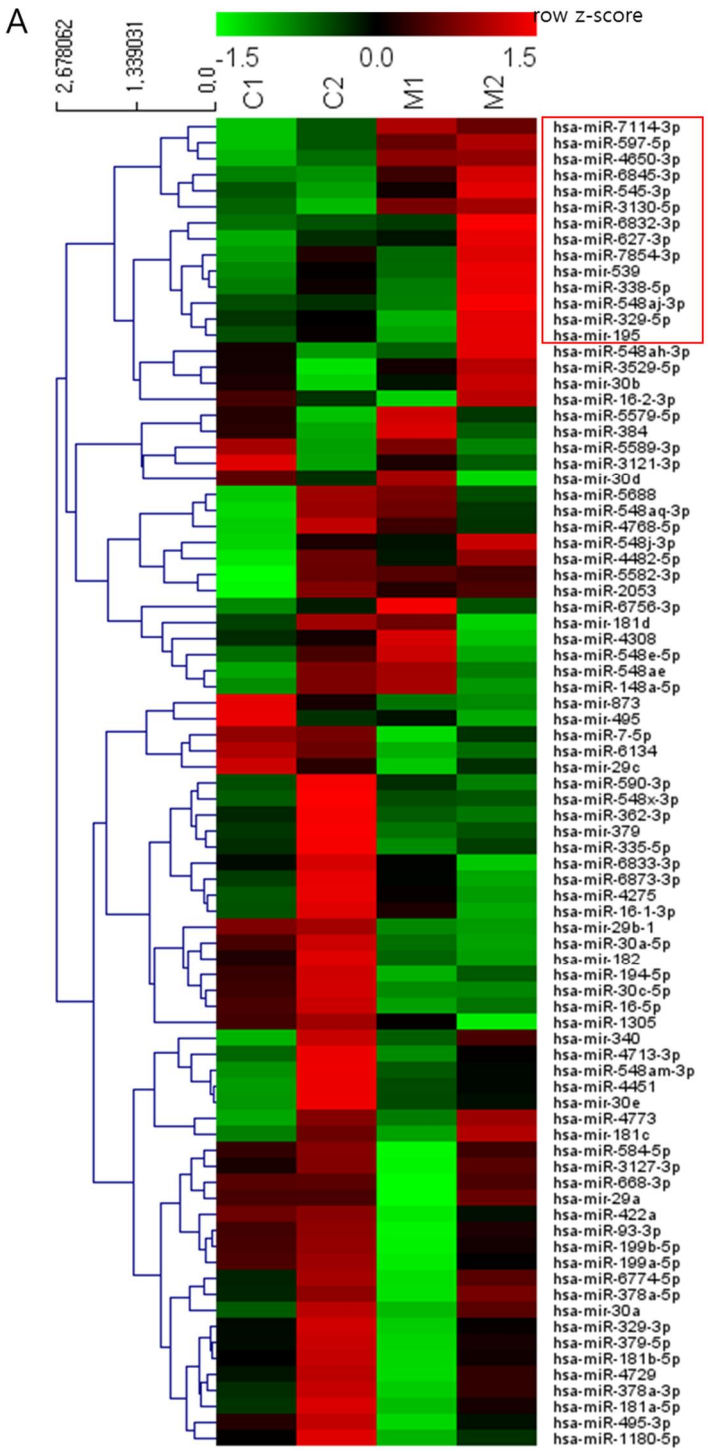
A
row z-score
-1.5
0.0
1.5
2.678062
1.339031
0.0
C1
C2
M1
M2
hsa-miR-7114-3p
hsa-miR-597-5p
hsa-miR-4650-3p
hsa-miR-6845-3p
hsa-miR-545-3p
hsa-miR-3130-5p
hsa-miR-6832-3p
hsa-miR-627-3p
hsa-miR-7854-3p
hsa-mir-539
hsa-miR-338-5p
hsa-miR-548aj-3p
hsa-miR-329-5p
hsa-mir-195
hsa-miR-548ah-3p
hsa-miR-3529-5p
hsa-mir-30b
hsa-miR-16-2-3p
hsa-miR-5579-5p
hsa-miR-384
hsa-miR-5589-3p
hsa-miR-3121-3p
hsa-mir-30d
hsa-miR-5688
hsa-miR-548aq-3p
hsa-miR-4768-5p
hsa-miR-548j-3p
hsa-miR-4482-5p
hsa-miR-5582-3p
hsa-miR-2053
hsa-miR-6756-3p
hsa-mir-181d
hsa-miR-4308
hsa-miR-548e-5p
hsa-miR-548ae
hsa-miR-148a-5p
hsa-mir-873
hsa-mir-495
hsa-miR-7-5p
hsa-miR-6134
hsa-mir-29c
hsa-miR-590-3p
hsa-miR-548x-3p
hsa-miR-362-3p
hsa-mir-379
hsa-miR-335-5p
hsa-miR-6833-3p
hsa-miR-6873-3p
hsa-miR-4275
hsa-miR-16-1-3p
hsa-mir-29b-1
hsa-miR-30a-5p
hsa-mir-182
hsa-miR-194-5p
hsa-miR-30c-5p
hsa-miR-16-5p
hsa-miR-1305
hsa-mir-340
hsa-miR-4713-3p
hsa-miR-548am-3p
hsa-miR-4451
hsa-mir-30e
hsa-miR-4773
hsa-mir-181c
hsa-miR-584-5p
hsa-miR-3127-3p
hsa-miR-668-3p
hsa-mir-29a
hsa-miR-422a
hsa-miR-93-3p
hsa-miR-199b-5p
hsa-miR-199a-5p
hsa-miR-6774-5p
hsa-miR-378a-5p
hsa-mir-30a
hsa-miR-329-3p
hsa-miR-379-5p
hsa-miR-181b-5p
hsa-miR-4729
hsa-miR-378a-3p
hsa-miR-181a-5p
hsa-miR-495-3p
hsa-miR-1180-5p

B

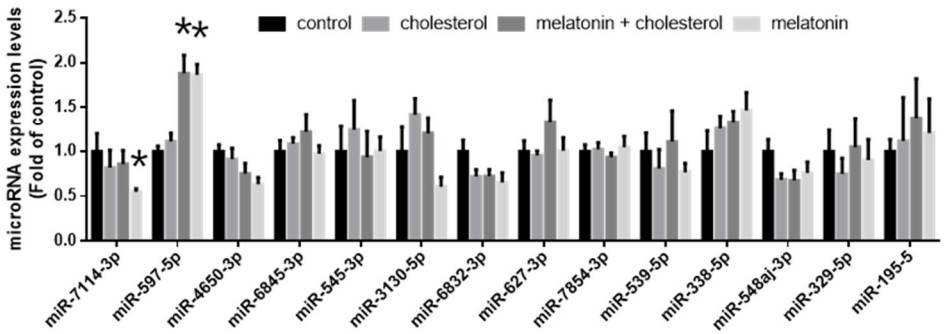

Figure 17. The changes in expression levels of BiP targeting microRNAs by melatonin and cholesterol treatment. UCB-MSCs were treated with melatonin (1 μM, 24 h) and total RNAs were extracted. 83 BiP-targeting microRNAs were selected from three databases (Genecards, microRNA.org, and Diana tools) and microRNA microarray was conducted. The expression levels of microRNAs were analyzed using hierarchical clustering with heatmap. (B) A cluster of expression-increased microRNAs was selected and their expression levels under high cholesterol (200 μM, 24 h) and melatonin (1 μM) condition were analyzed by qPCR (n=5, One-way ANOVA, $*p < 0.05$ vs control). Quantitative data are presented as a mean ± standard error of the mean.

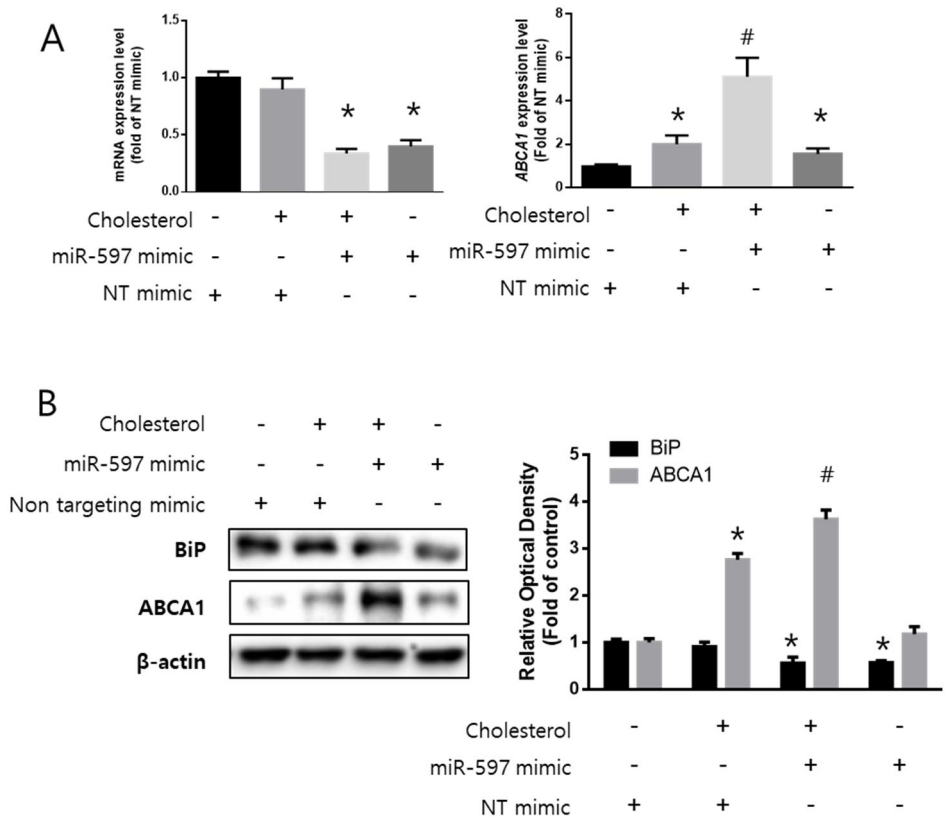

Figure 18. Effects of miR-597-5p on the expression of BiP and ABCA1. (A) miR-597 mimic was transfected to UCB-MSCs for 24 h prior to cholesterol treatment (200 μM, 12 h). The mRNA expressions of *HSPA5* and *ABCA1* were quantified with qPCR (n=5, One-way ANOVA, $*p < 0.05$ vs NT mimic, $\#p < 0.05$ vs NT mimic + cholesterol). (B) miR-597 mimic was transfected to UCB-MSCs for 24 h prior to cholesterol treatment (200 μM, 24 h). The expression levels of BiP and ABCA1 were measured with western blotting (n=5, One-way ANOVA, $*p < 0.05$ vs NT mimic, $\#p < 0.05$ vs NT mimic + cholesterol). All images are representative and quantitative data are presented as a mean ± standard error of the mean.

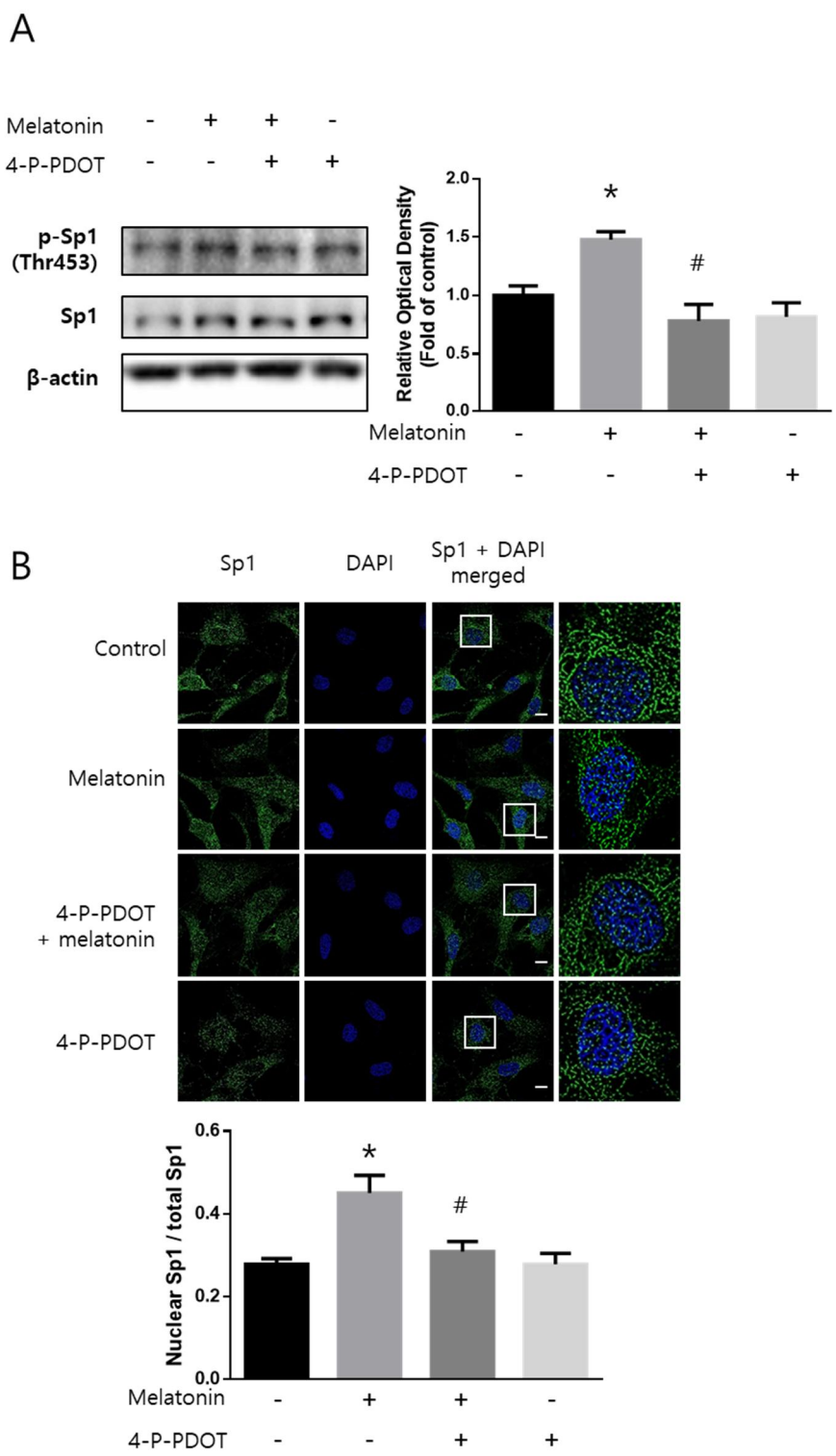
A
Melatonin - + + -
4-P-PDOT - - + +
p-Sp1 (Thr453)
Sp1
β-actin
Relative Optical Density (Fold of control)
2.0
1.5
1.0
0.5
0.0
*
#
Melatonin - + + -
4-P-PDOT - - + +
B
Sp1
DAPI
Sp1 + DAPI merged
Control
Melatonin
4-P-PDOT + melatonin
4-P-PDOT
Nuclear Sp1 / total Sp1
0.6
0.4
0.2
0.0
*
#
Melatonin - + + -
4-P-PDOT - - + +

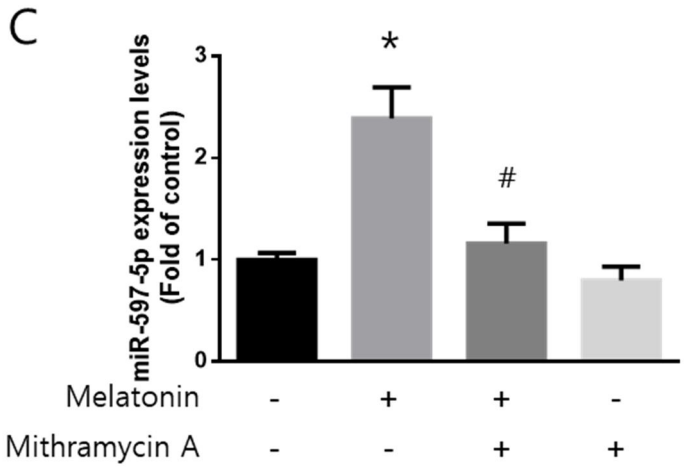

Figure 19. Role of melatonin-activated Sp1 on the expression of miR-597-5p. MT2 inhibitor 4-P-PDOT (10 μM) was pretreated for 30 min prior to melatonin treatment (1 μM, 12 h). (A) The phosphorylation of Sp1 (Thr453) were measured by western blotting (n=5, One-way ANOVA, $*p < 0.05$ vs control, $\#p < 0.05$ vs melatonin). (B) Immunocytochemistry was conducted with Sp1 (green) specific antibody and DAPI (blue) and then visualized by SRRF imaging system. Scale bar was set as 8 μm (Magnification ×1,000). The nuclear translocation of Sp1 was analyzed with Fiji software. Nuclear translocation of Sp1 was analyzed by ratio of nuclear Sp1 to total Sp1 (n=5, One-way ANOVA, $*p < 0.05$ vs control, $\#p < 0.05$ vs melatonin). (C) Sp1 inhibitor Mithramycin A (5 nM) was pretreated for 30 min prior to melatonin treatment (1 μM, 12 h), and the change of expression level of miR-597-5p was assessed through qPCR (n=5, One-way ANOVA, $*p < 0.05$ vs control, $\#p < 0.05$ vs melatonin). All images are representative and quantitative data are presented as a mean ± standard error of the mean.

DISCUSSION

Here, I demonstrate that melatonin protected UCB-MSCs from cholesterol-induced apoptosis through a BiP/NRF1-dependent intracellular cholesterol efflux mechanism. In the presence of high cholesterol levels, LXR α -dependent responses sense and adapt to increased cholesterol efflux through the increased expression of ABCA1 (Castrillo & Tontonoz, 2004; Festa et al., 2006; Kaneko et al., 2015). I show here that ABCA1 was required for the downregulation of intracellular cholesterol levels and cholesterol-induced apoptosis. Further, increased levels of ABCA1 in the presence of high cholesterol concentrations did not protect the cells from cholesterol-induced apoptosis. Previous studies showed that increasing the expression levels of cholesterol transporters upregulates cholesterol efflux, which is required for inhibiting cholesterol-induced apoptosis (Adorni et al., 2017; Zeng et al., 2018). Further, another study demonstrated that the overexpression of ABCA1 suppresses the accumulation of cholesterol (Stamatikos et al., 2019). In the present study, the melatonin treatment of UCB-MSCs reduced the levels of high-cholesterol-induced ROS and apoptosis as well as intracellular cholesterol levels by increasing the expression levels of ABCA1. As shown here and other studies, DIDS treatment with melatonin abolished cholesterol efflux mediated by ABCA1 without significantly changing the levels of ABCA1 or ROS (Di et al., 2012; Hou et al., 2007). This finding indicates that the protective effect of melatonin on high-cholesterol-induced ROS generation and apoptosis does not absolutely require scavenging of

ROS, but rather inhibition of cholesterol accumulation. Therefore, I suggest the protective effect conferred upon stem cells by melatonin is explained by ABCA1-mediated removal of ROS generated in response to excess levels of cholesterol.

Because of its occurrence and cost, skin wounds are main health concern and therapeutic approaches using UCB-MSCs have been conducted to accelerate the wound healing process in preclinical and clinical studies (Brown et al., 2019; Kasuya & Tokura, 2014). However, there are many reports that the effect of stem cell transplantation for promoting skin wound recovery was reduced in obese patients. (Awad et al., 2005; Schatteman & Ma, 2006) In obesity, impairment of skin wound recovery can lead to tissue necrosis, which can lead to not only a decrease in the patient's quality of life but also a threat from complications. (Pence & Woods, 2014) Therefore, I conducted this study for improving the efficacy of UCB-MSCs transplantation therapy in obese conditions, and the tissue regenerative effects were evaluated using the skin wound healing model. I showed that in a mouse model of obesity, melatonin treatment improved the efficacy of stem cell transplantation therapy using UCB-MSC, which was abolished by inhibiting of ABCA1. Melatonin did not significantly change the levels of plasma cholesterol of these mice, and analysis of the UCB-MSCs revealed a regulatory role that controls intracellular cholesterol levels. Previous investigations found that the administration of melatonin (10□ 30 mg/kg/day) for 4 to 8 weeks decreases total serum levels of cholesterol in sera harvested from HFD mice (de Farias et al., 2019; Li et al., 2019a; Ou et al., 2019). In the present study, melatonin (30 mg/kg/day) was injected for 12 days after wound formation. Consistent with this data, two other reports found that the

administration of melatonin (4□10 mg/kg/day) for two weeks had no significant effect on serum cholesterol levels (Salmanoglu et al., 2016; Yildirim et al., 2019). These differences can be attributed to the duration of melatonin administration. When focused on short-term treatment, melatonin affected the regulation of intracellular cholesterol levels in transplanted UCB-MSCs, rather than cholesterol levels in the blood. This study suggested that the decreased stem cell therapeutic efficacy in obese conditions was improved by an increase in survival rates of transplanted UCB-MSCs with melatonin treatment, although the plasma cholesterol levels in obese mice are still high, which can lead to disease onset. Other studies showed that melatonin treatment increases the efficacy of transplanted UCB-MSCs in skin wound healing experiments, while melatonin enhances immunoregulatory effects and the proliferation of adipose tissue-derived MSCs (Heo et al., 2019; Lee et al., 2014). In contrast, I show here that inhibition of ABCA1 expression diminished the effects of melatonin on the engraftment rate of UCB-MSCs and skin wound healing, which indicates that the regulation of intracellular cholesterol levels is an important role played by melatonin in this obese mouse model. Moreover, others found that the increased survival rate of transplanted UCB-MSCs positively correlates with their regenerative potentials, such as wound regeneration, wound-closing rate, and neovascularization (Lee et al., 2019; Oh et al., 2019). Together, these findings indicate that melatonin protects engrafted UCB-MSCs from apoptosis to increase the efficacy of wound healing. Therefore, melatonin treatment represents a potentially effective strategy for improving the efficacy of stem cell transplantation therapy.

I demonstrate here that melatonin decreased BiP expression through an MT2-dependent miR-597 regulatory pathway and that BiP is required for the nuclear translocation of NRF1, which regulates the expression of ABCA1. NRF1 is reported that regulates the antioxidant effect by increasing the transcription of antioxidant response element genes while regulating mitochondrial functions by increasing of mitophagy-related gene expression. (Biswas & Chan, 2010; Lee et al., 2018a; Yang et al., 2018) Under high cholesterol conditions, in contrast, NRF1 regulates cholesterol homeostasis in the ER membrane by decreasing the nuclear translocation while increasing the expression level of ABCA1. (Widenmaier et al., 2017) In addition, results of ROS showed that the decrease in high-cholesterol-induced ROS following melatonin treatment is ABCA1-dependent (Fig. 2D). Therefore, I investigated the role of NRF1 regulation by melatonin in ABCA1 expression under cholesterol conditions. In addition, cholesterol treatment increased the expression of MT2 in UCB-MSCs, and others found that ROS accumulation is significantly associated with MT2 expression (Lee et al., 2010; Onphachanh et al., 2017). I suggest, therefore, that high-cholesterol-induced ROS accumulation induces MT2 expression. If true, this process has important implications for using melatonin to control the levels of intracellular cholesterol because increased sensitivity to melatonin activates downstream pathways in the presence of high levels of cholesterol. Evidence indicates that BiP contributes to ERAD through the selection of substrates and assembly of the ERAD complex (Hosokawa et al., 2008; Wang et al., 2017). The ubiquitin-conjugating enzyme E2G2, together with the HRD1 complex, polyubiquitinates substrates and the valosin-containing protein (p97) to retro-transport substrates to the cytosol

(Spandl et al., 2011; Ye et al., 2003). The expression levels and translocation of NRF1 are regulated by ERAD, suggesting the participation of BiP in the ERAD-dependent translocation of NRF1 (Sykiotis & Bohmann, 2010). Present results are consistent with this possibility because I showed that inhibiting BiP further decreased the cholesterol-induced reduction in the nuclear translocation of NRF1, leading to increased expression of ABCA1. Numerous studies showed that melatonin treatments reduce stress-induced BiP expression (Lin et al., 2007; San-Miguel et al., 2014; Yoo et al., 2016). In present data, melatonin treatment decreased the levels of *HSPA5* mRNA and BiP but did not change the expression and activation of its transcription factor. Recent studies showed that melatonin regulates cellular physiological functions through microRNAs (Stacchiotti et al., 2019; Xia et al., 2019; Zhang et al., 2019). Further, microRNAs inhibit the proliferation and metastasis of cancer cells, and melatonin-induced miR-392a and miR-34b increase apoptosis of cancer cells through inhibition of ABCB1/ABCB4 activity (Chen et al., 2019; Hsieh et al., 2020; Li et al., 2019c; Zhang et al., 2018). Moreover, melatonin regulates the transcription of microRNAs through the CEBP pathway or the Sp1 pathway (Li et al., 2019b; Yang et al., 2014; Zeng et al., 2020). I, therefore, focused on the regulatory effects of a melatonin-induced microRNA on *HSPA5* mRNA transcription. Here I show that melatonin treatment increased MT2-dependent phosphorylation and nuclear translocation of Sp1, which induced miR-597-5p expression to inhibit BiP. The present study is the first, to report that melatonin induces miR-597. Further studies are required to define the mechanism through which miR-597-5p regulates BiP expression.

In conclusion, I demonstrate here that melatonin rescued UCB-MSCs from high-cholesterol-induced apoptosis by downregulating the expression of BiP, as well as the nuclear translocation of NRF1, which play a significant role in the regulation of intracellular cholesterol levels (Fig. 20). This is the first report to reveal the novel role of melatonin in intracellular cholesterol efflux and the details of the underlying mechanism. I suggest focusing efforts to develop a new strategy that employs melatonin to enhance the resistance of the UCB-MSCs to high cholesterol levels to improve the efficacy of stem cell transplantation to treat obese patients.

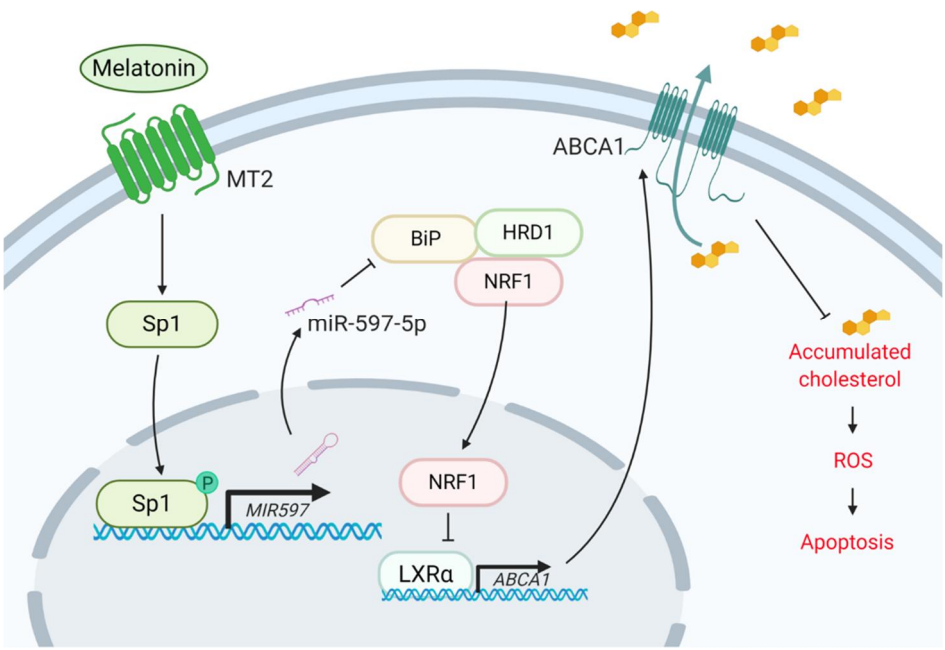

Figure 20. Schematic model of melatonin-induced cholesterol efflux and UCB-MSC survival through ABCA1 expression. Under high cholesterol conditions, the expression of MT2 increase and MT2-dependent melatonin signaling activates Sp1-dependent miR597 expression that suppresses the expression of BiP. Decreased BiP

results in inhibition of ERAD of NRF1 which responsible for translocation of NRF1. Inhibition of nuclear translocation of NRF1 resulted in LXRα-dependent expression of ABCA1, and then increases the efflux of intracellular cholesterol and inhibits cholesterol-induced ROS and apoptosis.

REFERENCES

Adorni, M. P., Cipollari, E., Favari, E., Zanotti, I., Zimetti, F., Corsini, A., Ricci, C., Bernini, F. & Ferri, N. (2017) Inhibitory effect of PCSK9 on Abca1 protein expression and cholesterol efflux in macrophages. Atherosclerosis, 256, 1-6.

Altunkaya, N., Erdogan, M. A., Ozgul, U., Sanli, M., Ucar, M., Ozhan, O., Sumer, F., Erdogan, S., Colak, C. & Durmus, M. (2018) Changes in melatonin, cortisol, and body temperature, and the relationship between endogenous melatonin levels and analgesia consumption in patients undergoing bariatric surgery. Obes Surg, 28(10), 3186-3192.

Avishai, E., Yeghiazaryan, K. & Golubnitschaja, O. (2017) Impaired wound healing: facts and hypotheses for multi-professional considerations in predictive, preventive and personalised medicine. EPMA J, 8(1), 23-33.

Awad, O., Jiao, C., Ma, N., Dunnwald, M. & Schatteman, G. C. (2005) Obese diabetic mouse environment differentially affects primitive and monocytic endothelial cell progenitors. Stem Cells, 23(4), 575-83.
Baron, K. G., Reid, K. J., Kim, T., Van Horn, L., Attarian, H., Wolfe, L., Siddique, J., Santostasi, G. & Zee, P. C. (2017) Circadian timing and alignment in healthy adults: associations with BMI, body fat, caloric intake and physical activity. Int J Obes (Lond), 41(2), 203-209.

Biswas, M. & Chan, J. Y. (2010) Role of Nrf1 in antioxidant response element-mediated gene expression and beyond. Toxicol Appl Pharmacol, 244(1), 16-20.

Brown, C., McKee, C., Bakshi, S., Walker, K., Hakman, E., Halassy, S., Svinarich, D., Dodds, R., Govind, C. K. & Chaudhry, G. R. (2019) Mesenchymal stem cells: Cell therapy and regeneration potential. J Tissue Eng Regen Med, 13(9), 1738-1755.

Castrillo, A. & Tontonoz, P. (2004) Nuclear receptors in macrophage biology: at the crossroads of lipid metabolism and inflammation. Annu Rev Cell Dev Biol, 20, 455-80.

Cheadle, C., Vawter, M. P., Freed, W. J. & Becker, K. G. (2003) Analysis of microarray data using Z score transformation. J Mol Diagn, 5(2), 73-81.

Chen, X., Zhang, C., Zhao, M., Shi, C. E., Zhu, R. M., Wang, H., Zhao, H., Wei, W., Li, J. B. & Xu, D. X. (2011) Melatonin alleviates lipopolysaccharide-induced hepatic SREBP-1c activation and lipid accumulation in mice. J Pineal Res, 51(4), 416-25.

Chen, Z., Ren, R., Wan, D., Wang, Y., Xue, X., Jiang, M., Shen, J., Han, Y., Liu, F., Shi, J., Kuang, Y., Li, W. & Zhi, Q. (2019) Hsa_circ_101555 functions as a competing endogenous RNA of miR-597-5p to promote colorectal cancer progression. Oncogene, 38(32), 6017-6034.

Choi, S. I., Lee, E., Akuzum, B., Jeong, J. B., Maeng, Y. S., Kim, T. I. & Kim, E. K. (2017) Melatonin reduces endoplasmic reticulum stress and corneal dystrophy-associated TGFBIp through activation of endoplasmic reticulum-associated protein degradation. J Pineal Res, 63(3).

de Farias, T., Cruz, M. M., de Sa, R., Severi, I., Perugini, J., Senzacqua, M., Cerutti, S. M., Giordano, A., Cinti, S. & Alonso-Vale, M. I. C. (2019) Melatonin supplementation decreases hypertrophic obesity and inflammation induced by high-fat diet in mice. Front Endocrinol, 10, 750.

Di, D., Wang, Z., Liu, Y., Luo, G., Shi, Y., Berggren-Soderlund, M., Nilsson-Ehle, P., Zhang, X. & Xu, N. (2012) ABCA1 upregulating apolipoproein M expression mediates via the RXR/LXR pathway in HepG2 cells. Biochem Biophys Res Commun, 421(1), 152-6.

Fang, J., Yan, Y., Teng, X., Wen, X., Li, N., Peng, S., Liu, W., Donadeu, F. X., Zhao, S. & Hua, J. (2018) Melatonin prevents senescence of canine adipose-derived mesenchymal stem cells through activating NRF2 and inhibiting ER stress. Aging (Albany NY), 10(10), 2954-2972.

Feng, B., Yao, P. M., Li, Y., Devlin, C. M., Zhang, D., Harding, H. P., Sweeney, M., Rong, J. X., Kuriakose, G., Fisher, E. A., Marks, A. R., Ron, D. & Tabas, I. (2003) The endoplasmic reticulum is the site of cholesterol-induced cytotoxicity in macrophages. Nat Cell Biol, 5(9), 781-92.

Festa, V., Cestino, L., Cavuoti, G., Soncini, S. & Festa, F. (2006) Recurrent groin hernia: a cognitive survey in Piedmont. Chir Ital, 58(1), 33-8.

Guo, S. & Dipietro, L. A. (2010) Factors affecting wound healing. J Dent Res, 89(3), 219-29.

Gupta, S., Raghuwanshi, N., Varshney, R., Banat, I. M., Srivastava, A. K., Pruthi, P. A. & Pruthi, V. (2017) Accelerated in vivo wound healing evaluation of microbial glycolipid containing ointment as a transdermal substitute. Biomed Pharmacother, 94, 1186-1196.

Gustafsson, N., Culley, S., Ashdown, G., Owen, D. M., Pereira, P. M. & Henriques, R. (2016) Fast live-cell conventional fluorophore nanoscopy with ImageJ through super-resolution radial fluctuations. Nat Commun, 7, 12471.

Heo, J. S., Pyo, S., Lim, J. Y., Yoon, D. W., Kim, B. Y., Kim, J. H., Kim, G. J., Lee, S. G. & Kim, J. (2019) Biological effects of melatonin on human adiposederived mesenchymal stem cells. Int J Mol Med, 44(6), 2234-2244.

Hosokawa, N., Wada, I., Nagasawa, K., Moriyama, T., Okawa, K. & Nagata, K. (2008) Human XTP3-B forms an endoplasmic reticulum quality control scaffold with the HRD1-SEL1L ubiquitin ligase complex and BiP. J Biol Chem, 283(30), 20914-24.

Hou, M., Xia, M., Zhu, H., Wang, Q., Li, Y., Xiao, Y., Zhao, T., Tang, Z., Ma, J. & Ling, W. (2007) Lysophosphatidylcholine promotes cholesterol efflux from mouse macrophage foam cells via PPARγ-LXRα-ABCA1-dependent pathway associated with apoE. Cell Biochem Funct, 25(1), 33-44.

Hsieh, M. J., Lin, C. W., Su, S. C., Reiter, R. J., Chen, A. W., Chen, M. K. & Yang, S. F. (2020) Effects of miR-34b/miR-892a upregulation and inhibition of ABCB1/ABCB4 on melatonin-induced apoptosis in

VCR-resistant oral cancer cells. Mol Ther Nucleic Acids, 19, 877-889.

Hsu, C. P., Lin, C. H. & Kuo, C. Y. (2018) Endothelial-cell inflammation and damage by reactive oxygen species are prevented by propofol via ABCA1-mediated cholesterol efflux. Int J Med Sci, 15(10), 978-985.
Hussain, S. A. (2007) Effect of melatonin on cholesterol absorption in rats. J Pineal Res, 42(3), 267-71.

Jung, J. A., Yoon, Y. D., Lee, H. W., Kang, S. R. & Han, S. K. (2018) Comparison of human umbilical cord blood-derived mesenchymal stem cells with healthy fibroblasts on wound-healing activity of diabetic fibroblasts. Int Wound J, 15(1), 133-139.

Kaneko, T., Kanno, C., Ichikawa-Tomikawa, N., Kashiwagi, K., Yaginuma, N., Ohkoshi, C., Tanaka, M., Sugino, T., Imura, T., Hasegawa, H. & Chiba, H. (2015) Liver X receptor reduces proliferation of human oral cancer cells by promoting cholesterol efflux via up-regulation of ABCA1 expression. Oncotarget, 6(32), 33345-57.

Karamitri, A. & Jockers, R. (2019) Melatonin in type 2 diabetes mellitus and obesity. Nat Rev Endocrinol, 15(2), 105-125.

Kasuya, A. & Tokura, Y. (2014) Attempts to accelerate wound healing. J Dermatol Sci, 76(3), 169-72.

Kedi, X., Ming, Y., Yongping, W., Yi, Y. & Xiaoxiang, Z. (2009) Free cholesterol overloading induced smooth muscle cells death and activated both ER- and mitochondrial-dependent death pathway. Atherosclerosis, 207(1), 123-30.

Kennaway, D. J. & Wright, H. (2002) Melatonin and circadian rhythms. Curr Top Med Chem, 2(2), 199-209.

Lee, C. H., Yoo, K. Y., Choi, J. H., Park, O. K., Hwang, I. K., Kwon, Y. G., Kim, Y. M. & Won, M. H. (2010) Melatonin's protective action against ischemic neuronal damage is associated with up-regulation of the MT2 melatonin receptor. J Neurosci Res, 88(12), 2630-40.

Lee, E.-b., Kim, G.-H. & Yoon, G. (2018a) Mitochondrial ROS regulates hepatoma cell invasiveness via NFE2L1. Free Radical Biology and Medicine, 120, S140.

Lee, H. J., Jung, Y. H., Oh, J. Y., Choi, G. E., Chae, C. W., Kim, J. S., Lim, J. R., Kim, S. Y., Lee, S. J., Seong, J. K. & Han, H. J. (2019) BICD1 mediates HIF1α nuclear translocation in mesenchymal stem cells during hypoxia adaptation. Cell Death Differ, 26(9), 1716-1734.

Lee, S., Jin, J. X., Taweechaipaisankul, A., Kim, G. A. & Lee, B. C. (2018b) Stimulatory effects of melatonin on porcine in vitro maturation are mediated by MT2 receptor. Int J Mol Sci, 19(6).

Lee, S. J., Jung, Y. H., Oh, S. Y., Yun, S. P. & Han, H. J. (2014) Melatonin enhances the human mesenchymal stem cells motility via melatonin receptor 2 coupling with Gαq in skin wound healing. J Pineal Res, 57(4), 393-407.

Li, D. J., Tong, J., Li, Y. H., Meng, H. B., Ji, Q. X., Zhang, G. Y., Zhu, J. H., Zhang, W. J., Zeng, F. Y., Huang, G., Hua, X., Shen, F. M. & Wang, P. (2019a) Melatonin safeguards against fatty liver by antagonizing TRAFs-mediated ASK1 deubiquitination and stabilization in a β-arrestin-1 dependent manner. J Pineal Res, 67(4), e12611.

Li, L., Qiu, X., Sun, Y., Zhang, N. & Wang, L. (2019b) SP1-stimulated miR-545-3p inhibits osteogenesis via targeting LRP5-activated Wnt/β-catenin signaling. Biochem Biophys Res Commun, 517(1), 103-110.

Li, S., Liu, Z., Fang, X. D., Wang, X. Y. & Fei, B. Y. (2019c) MicroRNA (miR)-597-5p inhibits colon cancer cell migration and invasion by targeting fos-like antigen 2 (FOSL2). Front Oncol, 9, 495.

Lin, A. M., Fang, S. F., Chao, P. L. & Yang, C. H. (2007) Melatonin attenuates arsenite-induced apoptosis in rat brain: involvement of mitochondrial and endoplasmic reticulum pathways and aggregation of α-synuclein. J Pineal Res, 43(2), 163-71.

Masson-Meyers, D. S., Andrade, T. A. M., Caetano, G. F., Guimaraes, F. R., Leite, M. N., Leite, S. N. & Frade, M. A. C. (2020) Experimental models and methods for cutaneous wound healing assessment. Int J Exp Pathol, 101(1-2), 21-37.

Mi, Y., Tan, D., He, Y., Zhou, X., Zhou, Q. & Ji, S. (2018) Melatonin modulates lipid metabolism in HepG2 cells cultured in high concentrations of oleic acid: AMPK pathway activation may play an important role. Cell Biochem Biophys, 76(4), 463-470.

Naji, A., Eitoku, M., Favier, B., Deschaseaux, F., Rouas-Freiss, N. & Suganuma, N. (2019) Biological functions of mesenchymal stem cells and clinical implications. Cell Mol Life Sci, 76(17), 3323-3348.

Nascimento, A. P. & Costa, A. M. (2006) Overweight induced by high-fat diet delays rat cutaneous wound healing. Br J Nutr, 96(6), 1069-77.

Oh, J. Y., Choi, G. E., Lee, H. J., Jung, Y. H., Chae, C. W., Kim, J. S., Lee, C. K. & Han, H. J. (2019) 17β-Estradiol protects mesenchymal stem cells against high glucose-induced mitochondrial oxidants production via Nrf2/Sirt3/MnSOD signaling. Free Radic Biol Med, 130, 328-342.

Onphachanh, X., Lee, H. J., Lim, J. R., Jung, Y. H., Kim, J. S., Chae, C. W., Lee, S. J., Gabr, A. A. & Han, H. J. (2017) Enhancement of high glucose-induced PINK1 expression by melatonin stimulates neuronal cell survival: Involvement of MT2/Akt/NF-κB pathway. J Pineal Res, 63(2).

Ou, T. H., Tung, Y. T., Yang, T. H. & Chien, Y. W. (2019) Melatonin improves fatty liver syndrome by inhibiting the lipogenesis pathway in hamsters with high-fat diet-induced hyperlipidemia. Nutrients, 11(4), 748.

Parfejevs, V., Debbache, J., Shakhova, O., Schaefer, S. M., Glausch, M., Wegner, M., Suter, U., Riekstina, U., Werner, S. & Sommer, L. (2018) Injury-activated glial cells promote wound healing of the adult skin in mice. Nat Commun, 9(1), 236.

Pence, B. D. & Woods, J. A. (2014) Exercise, Obesity, and Cutaneous Wound Healing: Evidence from Rodent and Human Studies. Adv Wound Care (New Rochelle), 3(1), 71-79.

Preston, G. M. & Brodsky, J. L. (2017) The evolving role of ubiquitin modification in endoplasmic reticulum-associated degradation. Biochem J, 474(4), 445-469.

Salmanoglu, D. S., Gurpinar, T., Vural, K., Ekerbicer, N., Dariverenli, E. & Var, A. (2016) Melatonin and L-carnitin improves endothelial disfunction and oxidative stress in Type 2 diabetic rats. Redox Biol, 8, 199-204.

San-Miguel, B., Crespo, I., Vallejo, D., Alvarez, M., Prieto, J., Gonzalez-Gallego, J. & Tunon, M. J. (2014) Melatonin modulates the autophagic response in acute liver failure induced by the rabbit hemorrhagic disease virus. J Pineal Res, 56(3), 313-21.

Schatteman, G. C. & Ma, N. (2006) Old bone marrow cells inhibit skin wound vascularization. Stem Cells, 24(3), 717-21.

Schindelin, J., Arganda-Carreras, I., Frise, E., Kaynig, V., Longair, M., Pietzsch, T., Preibisch, S., Rueden, C., Saalfeld, S., Schmid, B., Tinevez, J. Y., White, D. J., Hartenstein, V., Eliceiri, K., Tomancak, P. & Cardona, A. (2012) Fiji: an open-source platform for biological-image analysis. Nat Methods, 9(7), 676-82.

Schmitz, G., Langmann, T. & Heimerl, S. (2001) Role of ABCG1 and other ABCG family members in lipid metabolism. J Lipid Res, 42(10), 1513-20.

Sener, G., Balkan, J., Cevikbas, U., Keyer-Uysal, M. & Uysal, M. (2004) Melatonin reduces cholesterol accumulation and prooxidant state induced by high cholesterol diet in the plasma, the liver and probably in the aorta of C57BL/6J mice. J Pineal Res, 36(3), 212-6.

Spandl, J., Lohmann, D., Kuerschner, L., Moessinger, C. & Thiele, C. (2011) Ancient ubiquitous protein 1 (AUP1) localizes to lipid droplets and binds the E2 ubiquitin conjugase G2 (Ube2g2) via its G2 binding region. J Biol Chem, 286(7), 5599-606.

Stacchiotti, A., Grossi, I., Garcia-Gomez, R., Patel, G. A., Salvi, A., Lavazza, A., De Petro, G., Monsalve, M. & Rezzani, R. (2019) Melatonin effects on non-alcoholic fatty liver disease are related to microRNA-34a-5p/sirt1 axis and autophagy. Cells, 8(9), 1053.

Stamatikos, A., Dronadula, N., Ng, P., Palmer, D., Knight, E., Wacker, B. K., Tang, C., Kim, F. & Dichek, D. A. (2019) ABCA1 overexpression in endothelial cells in vitro enhances ApoAI-

mediated cholesterol efflux and decreases inflammation. Hum Gene Ther, 30(2), 236-248.

Strong, A. L., Neumeister, M. W. & Levi, B. (2017) Stem Cells and Tissue Engineering: Regeneration of the Skin and Its Contents. Clin Plast Surg, 44(3), 635-650.

Sykiotis, G. P. & Bohmann, D. (2010) Stress-activated cap'n'collar transcription factors in aging and human disease. Sci Signal, 3(112), re3.

Tabas, I. (2004) Apoptosis and plaque destabilization in atherosclerosis: the role of macrophage apoptosis induced by cholesterol. Cell Death Differ, 11 S12-S16.

Veghari, G., Sedaghat, M., Joshghani, H., Banihashem, S., Moharloei, P., Angizeh, A., Tazik, E. & Moghaddami, A. (2013) Obesity and risk of hypercholesterolemia in Iranian northern adults. ARYA Atheroscler, 9(1), 2-6.

Wang, W. F., Yan, L., Liu, Z., Liu, L. X., Lin, J., Liu, Z. Y., Chen, X. P., Zhang, W., Xu, Z. Z., Shi, T., Li, J. M., Zhao, Y. L., Meng, G., Xia, Y., Li, J. Y. & Zhu, J. (2017) HSP70-Hrd1 axis precludes the oncorepressor potential of N-terminal misfolded Blimp-1s in lymphoma cells. Nat Commun, 8(1), 363.

Widenmaier, S. B., Snyder, N. A., Nguyen, T. B., Arduini, A., Lee, G. Y., Arruda, A. P., Saksi, J., Bartelt, A. & Hotamisligil, G. S. (2017) NRF1 is an ER membrane sensor that is central to cholesterol homeostasis. Cell, 171(5), 1094-1109 e15.

Xia, Y., Chen, S., Zeng, S., Zhao, Y., Zhu, C., Deng, B., Zhu, G., Yin, Y., Wang, W., Hardeland, R. & Ren, W. (2019) Melatonin in macrophage biology: Current understanding and future perspectives. J Pineal Res, 66(2), e12547.

Yang, K., Huang, R., Fujihira, H., Suzuki, T. & Yan, N. (2018) N-glycanase NGLY1 regulates mitochondrial homeostasis and inflammation through NRF1. J Exp Med, 215(10), 2600-2616.

Yang, W. B., Chen, P. H., Hsu, T. s., Fu, T. F., Su, W. C., Liaw, H., Chang, W. C. & Hung, J. J. (2014) Sp1-mediated microRNA-182

expression regulates lung cancer progression. Oncotarget, 5(3), 740-53.

Ye, Y., Meyer, H. H. & Rapoport, T. A. (2003) Function of the p97-Ufd1-Npl4 complex in retrotranslocation from the ER to the cytosol: dual recognition of nonubiquitinated polypeptide segments and polyubiquitin chains. J Cell Biol, 162(1), 71-84.

Yildirim, A., Arabaci Tamer, S., Sahin, D., Bagriacik, F., Kahraman, M. M., Onur, N. D., Cayirli, Y. B., Cilingir Kaya, O. T., Aksu, B., Akdeniz, E., Yuksel, M., Cetinel, S. & Yegen, B. C. (2019) The effects of antibiotics and melatonin on hepato-intestinal inflammation and gut microbial dysbiosis induced by a short-term high-fat diet consumption in rats. Br J Nutr, 122(8), 841-855.

Yoo, Y. M., Han, T. Y. & Kim, H. S. (2016) Melatonin suppresses autophagy induced by clinostat in preosteoblast MC3T3-E1 cells. Int J Mol Sci, 17(4), 526.

Yvan-Charvet, L., Pagler, T. A., Seimon, T. A., Thorp, E., Welch, C. L., Witztum, J. L., Tabas, I. & Tall, A. R. (2010) ABCA1 and ABCG1 protect against oxidative stress-induced macrophage apoptosis during efferocytosis. Circ Res, 106(12), 1861-9.

Zeng, C., Sang, Y., Wang, F. Y. & Zhuang, S. M. (2020) Opposing roles of C/EBPα and eEF1A1 in Sp1-regulated miR-122 transcription. RNA Biol, 17(2), 202-210.

Zeng, Y., Peng, Y., Tang, K., Wang, Y. Q., Zhao, Z. Y., Wei, X. Y. & Xu, X. L. (2018) Dihydromyricetin ameliorates foam cell formation via LXRalpha-ABCA1/ABCG1-dependent cholesterol efflux in macrophages. Biomed Pharmacother, 101, 543-552.

Zhang, X. Y., Liu, D. J., Yuan, R. B., Zhang, D. H., Li, S. R., Zhang, S. H. & Zhang, L. Y. (2018) Low expression of miR-597 is correlated with tumor stage and poor outcome in breast cancer. Eur Rev Med Pharmacol Sci, 22(2), 456-460.

Zhang, Y., Lin, J., Zhou, X., Chen, X., Chen, A. C., Pi, B., Pan, G., Pei, M., Yang, H., Liu, T. & He, F. (2019) Melatonin prevents osteoarthritis-induced cartilage degradation via targeting microRNA-140. Oxid Med Cell Longev, 2019, 9705929.

Zhao, L., Chen, S., Yang, P., Cao, H. & Li, L. (2019) The role of mesenchymal stem cells in hematopoietic stem cell transplantation: prevention and treatment of graft-versus-host disease. Stem Cell Res Ther, 10(1), 182.

Zhu, Z., Li, R., Lv, Y. & Zeng, W. (2019) Melatonin protects rabbit spermatozoa from cryo-damage via decreasing oxidative stress. Cryobiology, 88, 1-8.

국 문 초 록

고콜레스테롤이 유도하는 중간엽 줄기세포 자멸사에 대한 멜라토닌의 보호 효과

서울대학교 대학원
수의학과 수의생명과학 전공
김 준 성
지도교수 한 호 재

제대혈 유래 중간엽 줄기세포 이식치료는 조직 재생을 촉진하기 위해 사용되고 있으며, 비만 환자에서 나타나는 이식치료 효율 저하는 고콜레스테롤 환경과 연관이 있다. 또한 세포 내 콜레스테롤 조절은 이식세포의 세포자멸사를 줄이는데 중요하다. 내분비 호르몬인 멜라토닌은 콜레스테롤 수준을 조절하는 것으로 보고되었으나 그 기전은 잘 알려져있지 않다. 따라서 이 연구는 멜라토닌의 콜레스테롤 유도성 세포사멸사 조절 기전을 규명하기 위해 수행되었다. 멜라토닌의 처리는 줄기세포의 콜레스테롤 수송단백질인 ABCA1 (ATP-binding cassette subfamily A member 1)의 발현을 증가시켜 세포 내 콜레스테롤 축적과 세포사멸을 감소시켰으며, ABCA1의 억제제 처리를 통해 멜라토닌의 보호효과가 ABCA1에 의한 것임을 확인하였다. 또한, 피부상처회복 모델을 이용하

여 멜라토닌의 처리가 비만쥐에서 나타나는 줄기세포 이식효율 감소를 정상화하는 것을 확인하였다. 고콜레스테롤 상황에서 줄기세포의 멜라토닌 수용체인 MT2의 발현이 증가하였고, 멜라토닌의 처리는 Sp1 전사인자를 통한 microRNA-597-5p의 발현 증가로 표적 단백질인 BiP (binding immunoglobulin protein)의 발현을 감소시켰다. 멜라토닌의 처리는 NRF1 (nuclear factor erythroid 2-related factor 1)의 핵내 이동에 필요한 BiP과 NRF1의 결합을 감소시켰으며, 이로 인한 NRF1의 핵내 이동 억제는 ABCA1 발현과 세포 내 콜레스테롤 배출을 증가시켜 고콜레스테롤에 의한 세포자멸사를 억제하였다. 결론적으로 멜라토닌은 MT2/BiP/NRF1 경로를 통해 ABCA1에 의한 세포내 콜레스테롤 배출을 증가시켜 고콜레스테롤에 의한 중간엽줄기세포의 세포자멸사를 감소시킨다.

주요어: 멜라토닌, 줄기세포 이식, 콜레스테롤, BiP, NFE2L1, ABCA1
학번: 2016-21752